Equivalent excitability through different sodium channel subtypes and implications for analgesia by subtype-selective drugs

Yu-Feng Xie[1], Jane Yang[1,2], Stéphanie Ratté[1], Steven A. Prescott[1,2,3]*

[1]Neurosciences and Mental Health, The Hospital for Sick Children, Toronto, ON, Canada
[2]Institute of Biomedical Engineering, University of Toronto, Toronto, ON, Canada
[3]Department of Physiology, University of Toronto, Toronto, ON, Canada

***Corresponding Author:** Steven A. Prescott (steve.prescott@sickkids.ca)

Short Title: Degenerate basis for nociceptor excitability

ABSTRACT

Nociceptive sensory neurons convey pain signals to the CNS. Nociceptor hyperexcitability amplifies those signals, causing pain hypersensitivity. Reducing nociceptor excitability should mitigate that hypersensitivity, consistent with the effects of loss-of-function mutations in voltage-gated sodium (Na_V) channels like $Na_V1.7$. Yet efforts to phenocopy such mutations pharmacologically have failed in clinical trials. This failure may stem from the degenerate nature of nociceptor excitability. Here, we show that nociceptors can achieve equivalent excitability using different combinations of $Na_V1.3$, $Na_V1.7$, and $Na_V1.8$. If $Na_V1.3$ and/or $Na_V1.8$ levels are high enough to maintain nociceptor excitability, selectively blocking $Na_V1.7$ (e.g. with PF-05089771) becomes inconsequential. We demonstrate shifts in drug efficacy by comparing neurons tested after different numbers of days in vitro (DIV): Nociceptor excitability relies on $Na_V1.8$ at DIV0 but that responsibility shifts to $Na_V1.7$ and $Na_V1.3$ on DIV4-7. A similar shift in Na_V-dependence occurs in vivo, following inflammation, and impacts the ability of PF-05089771 to modulate pain sensitivity. These results demonstrate that nociceptors are surprisingly flexible in using different Na_V isoforms to regulate excitability. This flexibility poses a serious problem for subtype-selective drugs whose efficacy hinges on such vagaries. Degeneracy at the cellular level must be considered when choosing drug targets at the molecular level.

INTRODUCTION

Chronic pain is an epidemic: It affects between 11 and 40% of the population worldwide based on recent estimates (1). Neuropathic pain, which arises from damage to the nervous system, is particularly hard to treat: Only 30% of those with neuropathic pain experience moderate (≥30%) relief using available treatments (2, 3). New treatments are needed but prospects are grim: A meagre 11% of analgesic drugs entering phase 1 trials are ultimately approved (4). This has triggered debate about why basic science discoveries are not yielding improved clinical outcomes (5). Suggested explanations include flaws in preclinical animal testing (6, 7) or clinical trial design (8) but biological explanations must also be considered. For example, degeneracy – the ability of a biological system to achieve equivalent function using different components (9) – complicates the modulation of neuronal excitability by enabling a drug targeting one ion channel to have its therapeutic effect subverted by changes in other ion channels (10).

Like nearly all neurons, primary nociceptive sensory neurons (nociceptors) rely on action potentials (spikes) to encode information. Their spike initiation properties (excitability) are thus critical for relaying nociceptive information to the CNS. Increasing nociceptor excitability amplifies the pain evoked by a given stimulus whereas decreasing nociceptor excitability attenuates that pain. It is, therefore, notable that nociceptor excitability is increased in many pathological pain conditions (11), and that the resulting increase in afferent activity may be necessary and sufficient to drive pathological pain (12–14). Neuronal excitability depends on the complex interplay between diverse ion channels (15–17) but some ion channels seem to be particularly important for pain. For instance, loss- or gain-of-function mutations in the gene *SCN9A*, which encodes the voltage-gated sodium channel $Na_V1.7$, cause loss of pain or painful neuropathies, respectively (18–21, for review see 22). Those mutations are associated with concordant changes in nociceptor excitability (23, 24), although other work has challenged the direct role of $Na_V1.7$, instead implicating increased opioid signaling (25, 26). Furthermore, in animal studies, nociceptor-specific deletion of $Na_V1.7$ abolished acute and inflammatory pain (27) yet neuropathic pain could still develop (28), consistent with a case report of neuropathic pain in a patient with congenital insensitivity to pain (29).

Notwithstanding potential concerns about $Na_V1.7$'s role in neuropathic pain, the prospect of phenocopying pain insensitivity by pharmacologically inhibiting $Na_V1.7$ channels spurred development of $Na_V1.7$-selective drugs (30–32). Supporting this strategy, the relatively selective expression of $Na_V1.7$ in peripheral neurons, especially in nociceptors (33–35), ought to minimize the risk of adverse effects. But despite much optimism, not a single $Na_V1.7$-selective inhibitor has passed phase 3 clinical trials (36, 37). Notably, most preclinical studies focussed on (or perhaps selectively reported) $Na_V1.7$-selective inhibitors reducing inflammatory pain, yet most clinical trials focussed on neuropathic pain. Even so, the disappointing results are hard to reconcile with the seemingly important role of $Na_V1.7$ in nociceptor excitability.

A serendipitous observation prompted us to reassess the role of $Na_V1.7$ in nociceptor excitability and the implications for analgesia. Specifically, we observed that tetrodotoxin (TTX), which inhibits $Na_V1.7$ and several other TTX-sensitive (TTX-S) Na_V channels, had variable effects, dramatically reducing nociceptor excitability in some conditions but not in others. This variability is consistent with degeneracy insofar as nociceptors may achieve equivalent excitability using different Na_V isoforms, some of which are TTX-resistant (TTX-R). We demonstrate here that the analgesic success of a $Na_V1.7$-selective inhibitor is indeed contingent on whether $Na_V1.7$ plays a dominant role in regulating nociceptor excitability.

RESULTS

Equivalent excitability can arise from different sodium channels

Small dorsal root ganglion (DRG) neurons (soma diameter <25 µm) tend to spike repetitively when depolarized by current injection (38). In our sample, most small neurons genetically identified as nociceptors (see Methods) spiked repetitively when tested 2-8 hours after dissociation (DIV0) or after 4-7 days in culture (DIV4-7), though the proportion of repetitively spiking neurons increased slightly over that interval (χ^2=4.51, p=0.034, chi-square test) (**Fig. 1A**). Strikingly, 100 nM TTX had no effect on the spiking pattern at DIV0 but converted all but one neuron to transient spiking at DIV4-7. Amongst neurons that spiked repetitively at baseline, TTX reduced the firing rate and increased rheobase only at DIV4-7 (**Fig. 1B**). TTX reduced spike height at DIV0 and DIV4-7, but more so at DIV4-7. There was a significant increase in capacitance and leak conductance density between DIV0 and DIV4-7, but no change in resting membrane potential (**Fig. 1C**). Normalizing leak conductance by capacitance (which increases over time because of neurite extension) is critical for disambiguating whether changes in input resistance reflect changes in cell size or membrane leakiness. Consistent with current clamp data, voltage clamp recordings showed that only a small fraction of sodium current is TTX-S at DIV0, whereas nearly all sodium current was blocked by TTX at DIV4-7 (**Fig. 1D**). Previous studies suggested that TTX-R channels play an important role in nociceptor excitability (39–41). Our initial results confirm this for DIV0 but show that their contribution diminishes after a few days in culture, with TTX-S channels becoming dominant by DIV4. Despite this dramatic reconfiguring of Na_V channels, excitability was remarkably stable, consistent with Flake et al. (42) who observed decreased TTX-R current and increased TTX-S current without a concomitant change in excitability following axotomy.

Different sodium channels control nociceptor excitability at DIV0 and DIV4-7

Next, we sought to identify the Na_V isoform responsible for repetitive spiking at each time point, starting with DIV0. Of the TTX-R Na_V channels expressed by nociceptors, $Na_V1.8$ has been implicated in repetitive spiking (40, 41). We measured sodium current in voltage clamp before and after applying the $Na_V1.8$-selective inhibitor PF-01247324 (PF-24) (43). At DIV0, 1 µM PF-24 abolished most of the sodium

current (**Fig. 2A**). The PF-24-sensitive current had slow inactivation kinetics, like the TTX-R current and unlike the fast TTX-S current in Figure 1D, and consistent with previous descriptions of $Na_V1.8$ (44). A different $Na_v1.8$ antagonist, A-803467, had a similar effect (**Fig. S1**). In current clamp, PF-24 converted 7 of 8 repetitively spiking neurons to transient spiking and significantly reduced evoked spiking (**Fig. 2B**). It also increased rheobase and decreased spike height but did not affect resting membrane potential (**Fig. 2C**). PF-24 had negligible effects when tested at DIV4-7 (**Fig. S2**). These results show that $Na_V1.8$ is the predominant Na_V isoform at DIV0 and is necessary for repetitive spiking at that time point. To test the sufficiency of $Na_V1.8$ to produce repetitive spiking, we tuned a conductance-based model neuron to reproduce DIV0 data described above (see Methods). In this DIV0 model, inclusion of $Na_V1.8$ conductance was sufficient to generate repetitive spiking (**Fig. 2D** left). The necessity of $Na_V1.8$ for repetitive spiking at DIV0 was also recapitulated: Despite some $Na_V1.7$ conductance, 85% reduction in the $Na_V1.8$ conductance converted spiking from repetitive to transient (**Fig. 2D** right and **Supplementary Table 1**).

Next, we sought to identify the Na_V isoform responsible for repetitive spiking at DIV4-7 using PF-05089771 (PF-71) to inhibit $Na_V1.7$ (45, 46) and ICA-121431 (ICA) to inhibit $Na_V1.1/1.3$ (47, 48). In voltage clamp, sodium current was significantly reduced by 30 nM PF-71, and most of the remaining current was blocked by 1 µM ICA (**Fig. 3A**). In current clamp, each inhibitor converted a significant proportion of neurons to transient spiking and significantly reduced firing rate (**Fig. 3B**). This argues that $Na_V1.7$ and $Na_V1.1/1.3$ are both necessary for repetitive spiking at DIV4-7. Inhibiting $Na_V1.7$ increased rheobase, unlike inhibiting $Na_V1.1/1.3$, and caused a stronger reduction in spike height (**Fig. 3C**). Neither affected resting membrane potential. These results show that $Na_V1.7$ is the predominant Na_V isoform at DIV4-7, but not the only one. PF-71 had minimal effects when tested at DIV0 (**Fig. S3**). We re-tuned our computational model to reproduce DIV4-7 data, with both $Na_V1.7$ and $Na_V1.3$ channels being required to produce repetitive spiking, meaning neither channel is individually sufficient (**Fig. 3D** and **Supplementary Table 1**). That said, inserting a higher density of either $Na_V1.7$ or $Na_V1.3$ could produce repetitive spiking in the absence of the other isoform (**Fig. S4**), consistent with $Na_V1.7$ and $Na_V1.3$ being functionally interchangeable, in the same way that $Na_V1.8$ and $Na_V1.7/1.3$ appear to be interchangeable.

Acutely interchanging Na_V isoforms does not affect spiking pattern

The ability of $Na_V1.3$, $Na_V1.7$ and $Na_V1.8$ to each encourage repetitive spiking is seemingly inconsistent with the common view that each Na_V isoform contributes selectively to a different phase of the spike (see Figure 3 in ref. 49). To test whether $Na_V1.7$ and $Na_V1.8$ currents are each sufficient to produce repetitive spiking, we asked whether the $Na_V1.8$ current necessary for spiking in our DIV0 model could be replaced with $Na_V1.7$, and whether the $Na_V1.7$ current necessary for spiking in our DIV4-7 model could be replaced with $Na_V1.8$. In both cases, repetitive spiking was restored after inserting the alternate current (**Fig. 4A**). We then proceeded with equivalent experiments in real neurons, inhibiting $Na_V1.8$ with PF-24 on DIV0 or $Na_V1.7$ with PF-71 on DIV4-7, and then introducing the alternate channel virtually using dynamic clamp (see *Methods*). The replacement was successful in all neurons tested (**Fig. 4B**). Inserting virtual $Na_V1.8$ after inhibiting native $Na_V1.8$ also restored repetitive spiking, and likewise for $Na_V1.7$ (**Fig. S5**), verifying that our virtual channels were indeed equivalent to the native channels we aimed to replace. Apart from maximal conductance densities, which was titrated in each neuron, all other parameters used for dynamic clamp were the same as for simulations. The success of these hybrid simulations helps validate our computational models insofar as simulated $Na_V1.7$ and $Na_V1.8$ currents interacted appropriately with native currents to produce repetitive spiking in real neurons, the same way they interact with other simulated currents in the model neuron.

With the model neurons thus validated, we used simulations to measure $Na_V1.7$ and $Na_V1.8$ currents during different phases of the spike. Notably, inward (depolarizing) current at voltages near spike threshold is critical for spike initiation (50) and it is, therefore, important to identify which Na_V isoform contributes to that current. In the DIV0 model, $Na_V1.7$ dominated during onset of the first spike but all subsequent spikes were initiated by $Na_V1.8$ (**Fig. 4C-D**). This occurred because the small $Na_V1.7$ conductance at DIV0 quickly inactivated during the first spike and remained inactive during subsequent spikes (**Fig. S6A**). This is consistent with experimental results, where repetitive spiking at DIV0 was unaffected by inhibiting $Na_V1.7$ (see Fig. S3) but was prevented by inhibiting $Na_V1.8$ (See Fig. 2). However, $Na_V1.7$ inactivation after the first spike was reflected by an increase in voltage threshold between the first

and second spike, both in the model (**Fig. 4C**) and in experiments (**Fig. S7**). This simulation result also predicted that TTX should affect the voltage threshold of the first spike in DIV0 neurons, despite not having other notable effects (see Fig. 1). As predicted, TTX caused a significant depolarizing shift in voltage threshold at DIV0 (**Fig. S8**), further validating our model. In the DIV4-7 model, $Na_V1.7$ and $Na_V1.3$ contributed to initiation of all spikes whereas $Na_V1.8$ was negligible **(Fig. 4E-F)**. Even though inactivation reduced $Na_V1.7$ current after the first spike (**Fig. S6B**), its total conductance at DIV4-7 was large enough that sufficient current remained to support repetitive spiking. Inactivation at DIV4-7 was reflected, however, in a combination of higher threshold and lower spike overshoot for the second spike, both in the model (**Fig. 4E-F**) and in experiments (**Fig. S7**). These results demonstrate that each Na_V isoform does not contribute exclusively to a particular phase of the spike, and nor is each spike phase mediated exclusively by a particular Na_V isoform; instead, each isoform contributes preferentially to a different spike phase depending on its voltage-dependency, but conductance density and inactivation status are both important. Indeed, an isoform's contribution can shift rapidly (because of channel inactivation) or slowly (because of gene expression changes).

Control of Na_V isoform expression differences between DIV0 and DIV4-7

Next, we sought to identify the basis for the slow shift in which Na_V isoform controls nociceptor excitability. **Figure 5A** shows mRNA levels for $Na_V1.7$ and $Na_V1.8$ relative to a housekeeping gene (left) and to each other (right). $Na_V1.7$ mRNA levels exceeded $Na_V1.8$ mRNA levels at both at both DIV0 and DIV7. Both decreased between DIV0 and DIV7, but $Na_V1.8$ more so, resulting in a significant decrease in the $Na_V1.8$:$Na_V1.7$ mRNA ratio. This pattern is consistent with the reduced role of $Na_V1.8$ at DIV4-7 but is inconsistent with the insignificant role of $Na_V1.7$ at DIV0; specifically, we expected $Na_V1.7$ mRNA levels to increase between DIV0 and DIV7. Next, we investigated if functional changes were better reflected by changes in protein levels. Immunofluorescence for $Na_V1.8$ was higher than for $Na_V1.7$ at DIV0, and that ratio reversed at DIV7 (**Fig. 5B**), consistent with functional changes. Moreover, cercosporamide (10 μM), a potent inhibitor of the eukaryotic translation Initiation Factor 4E (eIF4E), significantly mitigated the decrease in $Na_V1.8$ immunofluorescence and the increase in $Na_V1.7$ immunofluorescence when applied

to cultured neurons for 24 or 120 hours prior to measurements on DIV5 (**Fig. 5C**). Beyond showing that mRNA levels do not correlate well with Na_V isoform contributions to nociceptor excitability, reminiscent of some previous work (e.g. 51), these results suggest that translational regulation is crucial, though membrane trafficking and other processes may also contribute (52, 53).

Analgesic efficacy of subtype-selective drugs depends on which Na_V isoform controls nociceptor excitability

Since the analgesic effects of Na_V isoform-specific antagonists rely on modulating nociceptor excitability, analgesic efficacy hinges on nociceptor excitability being controlled by the targeted Na_V isoform. Accordingly, we predicted that the $Na_V1.7$-selective inhibitor PF-71 would have little if any effect on paw withdrawal under normal conditions, when $Na_V1.8$ controls nociceptor excitability (Figs. 2 and S3), but that it would be effective if $Na_V1.7$ took over control. Inflammation has been shown to increase $Na_V1.7$ channel trafficking and membrane expression (54–57). To test if inflammation increased $Na_V1.7$'s influence on nociceptor excitability, we recorded (on DIV0) from neurons cultured from mice whose hind paw was injected with CFA three days prior. Inflammation caused nociceptors innervating that paw to become much more variable in their reliance of specific Na_V isoforms (Fig. 6A). Inhibiting $Na_V1.7$ with PF-71 converted a significantly higher proportion of neurons to transient spiking after CFA (42%) than in control neurons (0%) (**Fig. 6B, left**), whereas subsequent application of PF-24 to inhibit $Na_V1.8$ converted just 14% of CFA neurons to transient spiking vs 88% of control neurons (**Fig 6B, right**). PF-71 also significantly affected resting membrane potential, rheobase, and spike height after CFA (**Fig. 6C**), unlike in control neurons (see Fig. S3). Overall, these results demonstrate that $Na_V1.7$ took on greater responsibility for nociceptor excitability after inflammation, which in turn predicts that PF-71 should reduce pain after inflammation but not under control conditions. As predicted, PF-71 significantly reduced thermal and tactile sensitivity in CFA-inflamed mice without having any effect in control mice (**Fig. 6D**). According to Nassar et al. (27) nociceptor-specific deletion of $Na_V1.7$ reduces thermal and tactile sensitivity in naïve mice; the inconsistency with our data argues that acute pharmacological inhibition of $Na_V1.7$ does not phenocopy chronic genetic manipulations.

DISCUSSION

Our results show that nociceptors can achieve similar excitability using different Na_V channels. Whereas repetitive spiking depends on $Na_V1.8$ shortly after dissociation (DIV0) and presumably under normal conditions in vivo, responsibility shifts to $Na_V1.7$ and $Na_V1.3$ after a few days in vitro (DIV4-7) due to translationally regulated changes in Na_V expression. Inflammation causes a similar shift in vivo. Importantly, inhibiting a particular Na_V isoform is consequential (analgesic) only if that isoform is responsible for nociceptor excitability (and only if nociceptors are responsible for the pain; see below). This may explain why $Na_V1.7$-selective drugs have not performed well in clinical trials – because $Na_V1.7$ is only sometimes necessary for nociceptor excitability depending on Na_V expression levels. Faster processes like channel inactivation also modulate the contribution of Na_V isoforms. These observations help explain inconsistencies at the root of poor reproducibility and translatability.

Contrary to the view that certain ion channels are uniquely responsible for certain aspects of neuronal function, neurons use diverse ion channel combinations to achieve similar function (58, 59). This degeneracy is crucial for enabling excitability and other aspects of neuron physiology to be homeostatically regulated by adjusting ion channels in response to perturbations (60–62). Degeneracy also enables pathological changes in different ion channels to produce equivalent hyperexcitability (63). This is important insofar as similar excitability may belie differences in the underlying ion channels – differences that may render a neuron susceptible or impervious to a drug depending on the functional necessity of the targeted ion channel in that neuron. This is precisely what our data demonstrate in nociceptors. Similar observations have been made in substantia nigra neurons, whose pacemaker activity can be mediated by Na_V channels or by voltage-gated calcium channels, meaning TTX may or may not block their spiking (64, 65). Similar interchangeability is evident for the burst firing of Purkinje neurons (66).

Degeneracy also exists at the circuit level (67, 68), where it allows differences in the intrinsic excitability of component neurons to be offset (and effectively hidden) by differences in synaptic weights (69). Relevant for pain processing, the spinal dorsal horn circuit can achieve similar output using different

synaptic weight combinations (70)2022-10-04 9:23:00 AM; specific neuron types may have a greater or lesser impact on circuit function depending on those weights. In effect, degeneracy introduces contingencies. The role of any ion channel in a neuron (or any neuron in a circuit) depends on the other ion channels in that neuron (or the synaptic connections with other neurons in the circuit). Because of such contingencies, a drug may engage its molecular target without producing the intended cellular, circuit or clinical effect. Indeed, different combinations of $GABA_A$ receptor activation and chloride driving force can produce equivalent synaptic inhibition (71), but when inhibition is incompensably compromised, the underlying cause necessitates different interventions (72). By this logic, if upregulation of $Na_V1.7$ is responsible for nociceptor hyperexcitability after nerve injury or inflammation, $Na_V1.7$ is an ideal target since "normal" neurons (not reliant on $Na_V1.7$) would be spared the effects of a $Na_V1.7$-selective drug, but the long-term efficacy of such a drug hinges on hyperexcitability remaining $Na_V1.7$-dependent, which cannot be assumed (10). Furthermore, if myelinated afferents (which express minimal $Na_V1.7$ (33)) are responsible for mechanical allodynia under neuropathic conditions (73–76), then $Na_V1.7$-selective drugs should not be expected to alleviate that symptom, which evidently they do not (77). Indeed, ablating nociceptors abolishes acute and inflammatory pain but not neuropathic pain (78, 79). Pathological pain being mediated by more than one afferent type is another example of circuit-level degeneracy.

Na_V isoforms must functionally overlap (80) in order to be interchangeable. Indeed, $Na_V1.8$ and $Na_V1.7$ are similar but not identical in their gating properties; for example, their voltage-dependencies partially overlap but the activation curve for $Na_V1.8$ is right-shifted compared to $Na_V1.7$ (81). Consequently, $Na_V1.7$ activates at voltages near threshold whereas $Na_V1.8$ tends to activate at suprathreshold voltages, during initiation and upstroke of the spike, respectively (36, 49). But that separation is not absolute. We found that $Na_V1.7$ contributes to initiation of the first spike in DIV0 neurons, but because it inactivates more readily than $Na_V1.8$, initiation of all subsequent spikes depends on $Na_V1.8$ (see Fig. 4), which activates at perithreshold voltages because voltage threshold is high (depolarized) in the absence of $Na_V1.7$. At DIV4-7, $Na_V1.7$ still inactivates (which causes voltage threshold to rise), but because of its higher density, it continues to produce enough inward current to continue to initiate later spikes. The activation pattern

we report for the first spike at DIV0 is consistent with Blair and Bean (82) who quantified the contribution of different Na_V channels by recording pharmacologically isolated currents while varying the holding potential according to the spike waveform. Our results go further in showing how responsibilities shift across different spikes within a train (because of differential Na_V inactivation) and across different conditions (because of changes in Na_V isoform expression).

With respect to reproducibility, labs testing nociceptors after different times in vitro would be expected to reach contradictory conclusions about the relative importance of a given Na_V isoform. Likewise, a testing protocol focusing on single spikes (the equivalent to the first spike in a train) would yield different results from one that considers repetitive spiking. Along the same lines, voltage clamp protocols that deliberately hold membrane potential at unnaturally hyperpolarized voltages to relieve inactivation before stepping up the voltage can give a misleading impression of how much a Na_V isoform contributes under natural conditions (i.e. with natural levels of inactivation). Such discrepancies might be chalked up to irreproducibility if the consequences of those methodological differences are not appreciated, especially if one overlooks how degeneracy allows responsibilities to shift between ion channels. Indeed, the pain literature is replete with apparent inconsistencies. We would argue that most of those studies are correct, but only under limited conditions; failure to identify and report those conditions (contingencies) represents a huge impediment to translation.

In summary, our results show that different Na_V isoforms can control the excitability of nociceptive sensory neurons. Responsibilities can shift on long and short timescales, yielding results that are seemingly inconsistent. By elucidating those shifting responsibilities using pharmacology, dynamic clamp and computational simulations, our results highlight the degenerate nature of nociceptor excitability. Degeneracy renders it impossible to claim without reservation that a particular Na_V isoform is uniquely responsible for pathological pain. Greater appreciation of degeneracy's implications would prompt better experimental design, more cautious interpretation, and, ultimately, improved translation.

MATERIALS AND METHODS

Animals

All animal procedures were approved by the Animal Care Committee at The Hospital for Sick Children and were conducted in accordance with guidelines from the Canadian Council on Animal Care. We used the Cre-*lox*P recombinase system to generate mice that express ChR2-eYFP in $Na_V1.8$-expressing neurons. Mice were obtained by crossing homozygous Ai32 mice (B6.Cg-Gt(ROSA)26Sortm32(CAG-COP4*H134R/EYFP)Hze/J) from Jax (#012569), which only express ChR2(H134R)-eYFP in the presence of Cre recombinase, with $Na_V1.8$-Cre mice (Tg(Scn10a-cre)1Rkun), which express Cre recombinase in $Na_v1.8$-expressing neurons (kindly provided by Rohini Kuner). The resulting mice express ChR2(H134R)-eYFP in $Na_V1.8$-expressing neurons. These neurons are primarily nociceptive and thermoreceptive (Agarwal et al, 2004). The $Na_V1.8$ promoter leads to transgene expression in >90% of neurons expressing markers of nociceptors (Nassar et al., 2004). To ensure that our transgenic mice were typical of wild-type mice with the same background (C57BL/6j), experiments reported in Fig. 1 were repeated in both genotypes for comparison. There was no effect of genotype on rheobase, spike height, input resistance, or spiking pattern, nor was there any significant interaction between genotype and effects of TTX except for spike height at DIV4-7, where TTX had a marginally larger effect in wild-type mice (Two-way ANOVA, $F_{1,54}$=4.968, p=0.03, see source data file); therefore, we pooled the data for Fig.1. Having verified that our foundational observations held across different genotypes, we proceeded to use transgenic mice for all subsequent experiments in order to identify eYFP-expressing nociceptors for patching, collection, or imaging.

Dorsal root ganglia neuron cultures

All key reagents are listed in **Supplementary Table 2**. Methods for primary DRG culture have been described previously (83). Briefly, adult mice (> 7 week-old) were anaesthetised with isoflurane and perfused intracardiacally with cold HBBS (without Ca and Mg, LifeTech 14170112) supplemented with (in mM) 15 HEPES, 28 Glucose, 111 sucrose, and pH adjusted with NaOH to 7.3-7.4; osmolarity 319-321. Lumbar dorsal root ganglia (DRGs) were extracted (L2-5, except for CFA-inflamed mice, in which we only took L4), digested with papain (Worthington Biochemical Corp.) and collagenase (Worthington

Biochemical Corp.)/dispase II (Sigma), and mechanically dissociated by trituration before being plated onto poly-D lysine-coated coverslips and incubated in a 50 μl droplet composed of Neurobasal™ media (Gibco 21103-049) supplemented with 1 % fetal bovine serum (FBS), B-27™ supplement (Thermo Fisher 17504-044) and 0.5mM L-Glutamine (Gibco 25030-081) for an initial period of 2 hours, allowing cells to attach to the glass coverslips. After this, the droplet was replaced with 1 ml of the same media. Cells were maintained in a 5% CO_2 incubator at 37°C. Media was changed every 3-4 days thereafter. Neurons were recorded at two time points after plating: 2-8 hours (referred to as DIV0) or 4-7 days (referred to as DIV4-7).

Electrophysiology

Coverslips with cultured neurons were transferred from the incubator to a recording chamber perfused with artificial cerebrospinal fluid containing (in mM): 126 NaCl, 2.5 KCl, 2.0 $CaCl_2$, 1.25 NaH_2PO_4, 26 $NaHCO_3$, 2 $MgCl_2$, and 10 glucose, bubbled with carbogen (5% CO_2:95% O_2) at room temperature. Neurons were visualized with gradient contrast optics on a Zeiss AxioExaminer microscope using a 40x, 0.75 NA water immersion objective (N-Achroplan, Zeiss) and IR-1000 Infrared CCD camera (Dage-MTI). YFP expression was visualized by epifluorescence (X-Cite, Excelitas) using a Zeiss filter set (46HE). A long-pass filter (OG590) was positioned in the transmitted light path to avoid activating ChR2 while patching. No optogenetic testing was performed as part of this study. Cells expressing YFP and with a soma diameter <25 μm were targeted for whole cell recording using pipettes (~5 MΩ resistance) pulled from borosilicate glass (WPI).

For current clamp recordings, pipettes were filled with intracellular solution containing (in Mm): 140 K-gluconate, 2 $MgCl_2$, 10 HEPES, 0.2 EGTA, 3.8 Na-ATP and 0.4 Na-GTP with pH adjusted to 7.3 with KOH; osmolarity was ~300 mOsm. A liquid junction potential correction of 15 mV was applied to all reported voltages. Series resistance was compensated to >70%. Signals were amplified with an Axopatch 200B amplifier (Molecular Devices, Sunnyvale, USA), low-pass filtered at 2 kHz, digitized with a Power1401 A/D device (Cambridge Electric Design, Cambridge, UK), and recorded at 10 kHz using CED software Signal version 6. After the natural resting membrane potential was noted, neurons were adjusted to -70 mV

using continuous current injection in current clamp mode. Action potentials (spikes) were evoked using a series of 1-second long depolarizing current injections. Rheobase was defined as the minimal current required to evoke a spike. Neurons were tested with current injections from 1x rheobase to 4x rheobase using increments of 0.5x rheobase. Repetitive spiking neurons were defined as those producing ≥3 spikes in response to any stimulus intensity; transient spiking neurons consistently produced ≤2 spikes. Spike threshold was defined as voltage where dV/dt first exceeds 5 mV/ms (84). Spike height was measured from threshold to peak of the action potential. Only neurons with a resting membrane potential below -35 mV, spikes overshooting 0 mV and recordings with <20% change in series resistance were tested and analyzed. For dynamic clamp experiments, the pipette shank was painted with Sylgard (Dow) to reduce pipette capacitance. Virtual $Na_V1.7$ and $Na_V1.8$ conductances were introduced into the cells using CED software Signal v6. Currents were defined using the Hodgkin-Huxley equation as in using the same parameter values as in our computational model (see below).

For voltage-clamp recordings, the bath solution was adjusted to reduce sodium currents to ensure proper clamping (85). Bath solution contained (in mM): 65 NaCl, 50 choline chloride, 5 KCl, 5 HEPES, 5 $MgCl_2$, 10 glucose, and 0.1 $CaCl_2$, plus 0.1 $CdCl_2$ to block calcium currents, and 20 TEA and 5 4-AP to block potassium currents; pH was adjusted to 7.4 with NaOH. Pipettes were filled with intracellular solution containing (in Mm): 140 CsCl, 10 HEPES, 2 $MgCl_2$, 1 EGTA, 3.8 Na-ATP, 0.4 Na-GTP; pH was adjusted to 7.3 with CsOH. The resulting pipette resistance was ~3 MΩ. A liquid junction potential correction of 4.8 mV was applied to all command voltages. Sodium currents were recorded during 20 ms-long steps from -85 mV to voltages between -45 and +15 mV (Gold et al., 1996). Series resistance was compensated to >80%. Signals were amplified, low-pass filtered at 5 kHz, and digitized as described for current clamp recordings.

Quantitative reverse transcription PCR (RT-qPCR)

Cultured DRG neurons <25 μm and expressing eYFP were identified as described above for patching. Coverslips were perfused with aCSF made with DEPC-treated ddH_2O, and identified neurons were collected using a glass pipette filled with intracellular solution also made from DEPC-treated ddH_2O

(composition otherwise the same as described above for electrophysiology). Approximately 50 neurons were collected at DIV0 and at DIV4-7. Total mRNA was extracted with a PureLink RNA mini kit after digestion of genomic DNA with DNase I (Thermo Fisher Scientific) and the cDNA was synthesized with a SuperScript II first-strand synthesis kit (Thermo Fisher Scientific) according to instructions. RT-qPCR was performed with the cDNA primers of target genes (**Supplementary Table 3**), and the PowerUp SYBR® Green master mix (Thermo Fisher Scientific) in the QuantStudio-3 real-time PCR system. The primers were designed with IDT and spanned at least one exon longer than 1000 bp in order to exclude contamination from genomic RNA. Non-RT mRNA was also used as a negative control to exclude contamination from genomic RNA. All target genes were performed in triplicate for each sample and the experiments were repeated at least 3 times. $Na_V1.7$ and $Na_V1.8$ transcript levels were analyzed using the 2-ΔΔCT method and compared with the housekeeping gene HPRT (Eissa et al., 2017; Fouillet et al., 2017).

Immunocytochemistry

Cultured DRG neurons were treated with 4% paraformaldehyde for 10 minutes, rinsed 3x with cold PBS, and permeabilized with 0.1% Triton X-100 in PBS. After another 3x rinse with PBS, neurons were treated with 10% normal goat serum for 30 min followed with rabbit primary $Na_V1.7$ antibody (1:200, ASC-008, Alomone) or $Na_V1.8$ antibody (1:200, ASC-028, Alomone) in PBS with 0.1% Tritween-20 and 1% BSA for 1 h. For some of the coverslips, primary antibodies were replaced with control peptides (ASC008AG1040 for $Na_V1.7$ and ASC016AG0640 for $Na_V1.8$) provided by Alomone as negative controls. Following 3x rinse in PBS, neurons were incubated in the dark with goat anti-rabbit secondary antibody Alexa Fluor-647 (1:500, Abcam) in PBS containing 1% BSA for 1 h, followed by DAPI staining for 10 min. All incubations were done at room temperature. Finally, coverslips were mounted on slides with mounting media (Abcam, ab128982), imaged with a spinning disk confocal microscope (Quorum Technologies) using the same acquisition setting across all imaging sessions, and analyzed with Volocity software (v6.5.1). Protein levels are measured using fluorescence intensity and expressed relative to each other (e.g. ratios in Fig 5C) or relative to fluorescence intensity for YFP in the same cells. Cell culture preparations and imaging were repeated in a minimum of 3 animals.

Behavioral testing

Behavioral tests were performed on adult mice (male and female, 8-12 weeks). Mice were acclimated to the testing environment for at least 1 h the day prior to start of experiments. Behavioral testing (von Frey test and Hargreaves test) was then performed for 2-3 consecutive days for baseline and for another 3 days after CFA injection. Behavioral tests were performed at the same time in the morning, at room temperature (21°C) following a one-hour acclimation period. Animals were randomly assigned to experimental groups and the experimenter was blind to the drug condition.

CFA injection. CFA (Sigma, F5881) was thoroughly dissolved in saline (1:1) by vortexing the mixture. The resulting CFA solution (20 µl) was injected subdermally into the left hind paw under light isoflurane anaesthesia. The injection was performed shortly after the last baseline test, on Day 0.

PF-71 administration. Injectable PF-71 solution was prepared by first dissolving PF-71 in DMSO to make a 5% stock solution; dissolution was achieved by heating to 37°C and vortexing. On the day of injection, stock solution was dissolved in sunflower oil (5% v/v) by sonicating for 5 min. Freshly prepared final PF-71 solution was injected intraperitoneally (1 g/kg body weight). Behavioral testing was performed 2 hours after injection of PF-71 or vehicle.

Von Frey testing. Mechanical hyperalgesia was assessed with von Frey filaments (North Coast) using the SUDO method (Bonin et al, 2014). The average of 3 trials in each animal was used for analysis.

Hargreaves testing. Thermal hyperalgesia was assessed with the Hargreaves apparatus (Ugo Basile, Italy). Radiant heating was applied to the plantar surface of the left hind paw. The interval between stimulus onset and paw withdrawal was defined as paw withdrawal latency (PWL). A 20 s cut-off was set to prevent damage to the skin if the animal failed to withdraw. The average of 3 trials in each animal was used for analysis.

Statistical analysis

Results are expressed as mean ± SEM when data are normally distributed or as median and quartiles

if non-normally distributed. Normality was tested using the Kolmogorov-Smirnov test. Analysis was performed with GraphPad Prism (v9) and SigmaPlot (v11). Normally distributed data were compared using t-tests or two-way ANOVAs followed by a Student Newman-Keuls post hoc test. Non-normally distributed data were compared using Mann-Whitney and Wilcoxon signed rank tests. Fisher exact and McNemar test were used for categorical data. Exact significance values and test results are reported throughout figure legends.

Computer model

Two separate, single compartmental models were built for DIV 0 and DIV4-7. They have the same, seven conductances: $g_{\mathrm{Nav1.3}}$, $g_{\mathrm{Nav1.7}}$, $g_{\mathrm{Nav1.8}}$, g_{Kdr}, g_{M}, g_{AHP} and g_{Leak}. Channel equations and their gating parameters are provided in **Supplementary Table 4**. Conductance densities at baseline (**Supplementary Table 5**) were tuned to qualitatively reproduce the changes in Na_V channel expressions at DIV 0 and 4-7 indicated by the experiments; changes to other channels were minimized between the two models. The effects of ICA, PF-71 and PF-24 were simulated by adjusting $\bar{g}_{\mathrm{Nav1.3}}$, $\bar{g}_{\mathrm{Nav1.7}}$ and $\bar{g}_{\mathrm{Nav1.8}}$, respectively, as reported in the figures. Channel noise was added as Ornstein-Uhlenbeck process with μ_{noise}= 0 $\mu\mathrm{A/cm^2}$, σ_{noise}= 0.05 $\mu\mathrm{A/cm^2}$, and τ = 5 ms. All computer code is available at ModelDB (http://modeldb.yale.edu/267560; restricted access until full publication).

CONTRIBUTIONS: YX, SR, SAP designed the research; YX, JY collected data, YX, JY, SR, SAP analyzed data; YX, SR, SAP wrote the manuscript.

ACKNOWLEDGMENTS: This work was supported by a Restracomp fellowship to JY and by a Canadian Institutes of Health Research Foundation Grant (FDN167276) to SAP. We thank Rohini Kuner for providing Na_v1.8-Cre mice, Jason Jeong and Russell Smith for expert technical assistance with animal care and cell cultures, and Yongqian Wang for advice on qPCR data acquisition.

REFERENCES

1. Cohen SP, Vase L, Hooten WM. Chronic pain: an update on burden, best practices, and new advances. *Lancet* 2021;397(10289):2082–2097.

2. Finnerup NB et al. Pharmacotherapy for neuropathic pain in adults: a systematic review and meta-analysis. *Lancet Neurol* 2015;14(2):162–173.

3. Rosenberger DC, Blechschmidt V, Timmerman H, Wolff A, Treede RD. Challenges of neuropathic pain: focus on diabetic neuropathy. *J Neural Transm* 2020;127(4):589–624.

4. Hay M, Thomas DW, Craighead JL, Economides C, Rosenthal J. Clinical development success rates for investigational drugs. *Nature Biotech* 2014;32(1):40–51.

5. Woolf CJ. Overcoming obstacles to developing new analgesics. *Nat Med* 2010;16(11):1241–1247.

6. Mogil JS. Animal models of pain: progress and challenges. *Nat Rev Neurosci* 2009;10(4):283–294.

7. Taneja A, Di Iorio VL, Danhof M, Della Pasqua O. Translation of drug effects from experimental models of neuropathic pain and analgesia to humans. *Drug Discov Today* 2012;17(15–16):837–849.

8. Mao J. Current challenges in translational pain research. *Trends Pharmacol Sci* 2012;33(11):568–573.

9. Edelman GM, Gally JA. Degeneracy and complexity in biological systems. *Proc Natl Acad Sci U S A* 2001;98(24):13763–13768.

10. Ratté S, Prescott SA. Afferent hyperexcitability in neuropathic pain and the inconvenient truth about its degeneracy. *Curr Opin Neurobiol* 2016;36:31–37.

11. Zhang JM, Song XJ, LaMotte RH. Enhanced excitability of sensory neurons in rats with cutaneous hyperalgesia produced by chronic compression of the dorsal root ganglion. *J Neurophysiol* 1999;82(6):3359–3366.

12. Gold MS, Gebhart GF. Nociceptor sensitization in pain pathogenesis. *Nat Med* 2010;16(11):1248–1257.

13. Haroutounian S et al. Primary afferent input critical for maintaining spontaneous pain in peripheral neuropathy. *Pain* 2014;155(7):1272–1279.

14. Yatziv S-L, Devor M. Suppression of neuropathic pain by selective silencing of dorsal root ganglion ectopia using nonblocking concentrations of lidocaine. *Pain* 2019;160(9):2105–2114.

15. Alles SRA, Smith PA. Peripheral voltage-gated cation channels in neuropathic pain and their potential as therapeutic targets. *Front Pain Res* 2021;2:750583.

16. Bean BP. The action potential in mammalian central neurons. *Nat Rev Neurosci* 2007;8(6):451–465.

17. Waxman SG, Zamponi GW. Regulating excitability of peripheral afferents: emerging ion channel targets. *Nat Neurosci* 2014;17(2):153–163.

18. Cox JJ et al. An SCN9A channelopathy causes congenital inability to experience pain. *Nature* 2006;444(7121):894–898.

19. Faber CG et al. Gain of function $Na_V1.7$ mutations in idiopathic small fiber neuropathy. *Ann Neurol* 2012;71(1):26–39.

20. Fertleman CR et al. SCN9A mutations in paroxysmal extreme pain disorder: allelic variants underlie distinct channel defects and phenotypes. *Neuron* 2006;52(5):767–774.

21. Yang Y et al. Mutations in SCN9A, encoding a sodium channel alpha subunit, in patients with primary erythermalgia. *J Med Gen* 2004;41(3):171–174.

22. Dib-Hajj SD, Yang Y, Black JA, Waxman SG. The $Na_V1.7$ sodium channel: from molecule to man. *Nat Rev Neurosci* 2013;14(1):49–62.

23. Cheng X et al. Deletion mutation of sodium channel $Na_V1.7$ in inherited erythromelalgia: enhanced slow inactivation modulates dorsal root ganglion neuron hyperexcitability. *Brain* 2011;134(Pt 7):1972–1986.

24. Dib-Hajj SD et al. Gain-of-function mutation in $Na_V1.7$ in familial erythromelalgia induces bursting of sensory neurons. *Brain* 2005;128(Pt 8):1847–1854.

25. MacDonald DI et al. A central mechanism of analgesia in mice and humans lacking the sodium channel $Na_V1.7$. *Neuron* 2021;109(9):1497-1512 e6.

26. Minett MS et al. Endogenous opioids contribute to insensitivity to pain in humans and mice lacking sodium channel $Na_V1.7$. *Nat Commun* 2015;6:8967.

27. Nassar MA et al. Nociceptor-specific gene deletion reveals a major role for $Na_V1.7$ (PN1) in acute and inflammatory pain. *Proc Natl Acad Sci U S A* 2004;101(34):12706–12711.

28. Nassar MA, Levato A, Stirling LC, Wood JN. Neuropathic pain develops normally in mice lacking both $Na_V1.7$ and $Na_V1.8$. *Mol Pain* 2005;1:24.

29. Wheeler DW, Lee MCH, Harrison EK, Menon DK, Woods CG. Case Report: Neuropathic pain in a patient with congenital insensitivity to pain. *F1000Research* 2014;3. doi:10.12688/f1000research.2642.2

30. Emery EC, Luiz AP, Wood JN. $Na_V1.7$ and other voltage-gated sodium channels as drug targets for pain relief. *Expert Opin Ther Targets* 2016;20(8):975–983.

31. Vetter I et al. $Na_V1.7$ as a pain target - From gene to pharmacology. *Pharmacol Ther* 2017;172:73–100.

32. Yang Y, Mis MA, Estacion M, Dib-Hajj SD, Waxman SG. $Na_V1.7$ as a pharmacogenomic target for pain: Moving toward precision medicine. *Trends Pharmacol Sci* 2018;39(3):258–275.

33. Djouhri L et al. Sensory and electrophysiological properties of guinea-pig sensory neurones expressing $Na_V1.7$ (PN1) Na^+ channel alpha subunit protein. *J Physiol* 2003;546(Pt 2):565–576.

34. Shiers SI et al. Convergence of peptidergic and non-peptidergic protein markers in the human dorsal root ganglion and spinal dorsal horn. *J Comp Neurol* 2021;529(10):2771–2788.

35. Toledo-Aral JJ et al. Identification of PN1, a predominant voltage-dependent sodium channel expressed principally in peripheral neurons. *Proc Natl Acad Sci U S A* 1997;94(4):1527–1532.

36. Alsaloum M, Higerd GP, Effraim PR, Waxman SG. Status of peripheral sodium channel blockers for non-addictive pain treatment. *Nat Rev Neurol* 2020;16(12):689–705.

37. Mulcahy JV et al. Challenges and opportunities for therapeutics targeting the voltage-gated sodium channel isoform $Na_V1.7$. *J Med Chem* 2019;62(19):8695–8710.

38. Amir R, Michaelis M, Devor M. Membrane potential oscillations in dorsal root ganglion neurons: role in normal electrogenesis and neuropathic pain. *J Neurosci* 1999;19(19):8589–8596.

39. Caffrey JM, Eng DL, Black JA, Waxman SG, Kocsis JD. Three types of sodium channels in adult rat dorsal root ganglion neurons. *Brain Res* 1992;592(1–2):283–297.

40. Renganathan M, Cummins TR, Waxman SG. Contribution of $Na_V1.8$ sodium channels to action potential electrogenesis in DRG neurons. *J Neurophysiol* 2001;86(2):629–640.

41. Rush AM, Cummins TR, Waxman SG. Multiple sodium channels and their roles in electrogenesis within dorsal root ganglion neurons. *J Physiol* 2007;579(Pt 1):1–14.

42. Flake NM, Lancaster E, Weinreich D, Gold MS. Absence of an association between axotomy-induced changes in sodium currents and excitability in DRG neurons from the adult rat. *Pain* 2004;109(3):471–480.

43. Payne CE et al. A novel selective and orally bioavailable $Na_V1.8$ channel blocker, PF-01247324, attenuates nociception and sensory neuron excitability. *Br J Pharmacol* 2015;172(10):2654–2670.

44. Vijayaragavan K, O'Leary ME, Chahine M. Gating properties of $Na_V1.7$ and $Na_V1.8$ peripheral nerve sodium channels. *J Neurosci* 2001;21(20):7909–7918.

45. Alexandrou AJ et al. Subtype-selective small molecule inhibitors reveal a fundamental role for $Na_V1.7$ in nociceptor electrogenesis, axonal conduction and presynaptic release. *PLoS One* 2016;11(4):e0152405.

46. Theile JW, Fuller MD, Chapman ML. The selective $Na_V1.7$ inhibitor, PF-05089771, interacts equivalently with fast and slow inactivated $Na_V1.7$ channels. *Mol Pharmacol* 2016;90(5):540–548.

47. McCormack K et al. Voltage sensor interaction site for selective small molecule inhibitors of voltage-gated sodium channels. *Proc Natl Acad Sci U S A* 2013;110(29):E2724–E2732.

48. Strege PR et al. Sodium channel $Na_V1.3$ is important for enterochromaffin cell excitability and serotonin release. *Sci Rep* 2017;7(1):15650.

49. Bennett DL, Clark AJ, Huang J, Waxman SG, Dib-Hajj SD. The role of voltage-gated sodium channels in pain signaling. *Physiol Rev* 2019;99(2):1079–1151.

50. Prescott SA, De Koninck Y, Sejnowski TJ. Biophysical basis for three distinct dynamical mechanisms of action potential initiation. *PLoS Comput Biol* 2008;4(10):e1000198.

51. Berta T et al. Transcriptional and functional profiles of voltage-gated Na^+ channels in injured and non-injured DRG neurons in the SNI model of neuropathic pain. *Mol Cell Neurosci* 2008;37(2):196–208.

52. Dustrude ET, Wilson SM, Ju W, Xiao Y, Khanna R. CRMP2 Protein SUMOylation Modulates $Na_V1.7$ Channel Trafficking. *J Biol Chem* 2013;288(34):24316–24331.

53. Yamane M et al. A functional coupling between CRMP1 and $Na_V1.7$ for retrograde propagation of Semaphorin3A signaling. *J Cell Sci* 2017;130(8):1393–1403.

54. Gould HJ, England JD, Liu ZP, Levinson SR. Rapid sodium channel augmentation in response to inflammation induced by complete Freund's adjuvant. *Brain Res* 1998;802(1–2):69–74.

55. Black JA, Liu S, Tanaka M, Cummins TR, Waxman SG. Changes in the expression of tetrodotoxin-sensitive sodium channels within dorsal root ganglia neurons in inflammatory pain. *Pain* 2004;108(3):237–247.

56. Liang L, Fan L, Tao B, Yaster M, Tao Y-X. Protein kinase B/Akt is required for complete Freund's adjuvant-induced upregulation of $Na_V1.7$ and $Na_V1.8$ in primary sensory neurons. *J Pain* 2013;14(6):638–647.

57. Akin EJ et al. Building sensory axons: Delivery and distribution of $Na_V1.7$ channels and effects of inflammatory mediators. *Sci Adv* 2019;5(10):eaax4755.

58. Marder E, Goaillard J-M. Variability, compensation and homeostasis in neuron and network function. *Nat Rev Neurosci* 2006;7(7):563–574.

59. O'Leary T, Williams AH, Franci A, Marder E. Cell types, network homeostasis, and pathological compensation from a biologically plausible ion channel expression model. *Neuron* 2014;82(4):809–821.

60. Drion G, O'Leary T, Marder E. Ion channel degeneracy enables robust and tunable neuronal firing rates. *Proc Natl Acad Sci U S A* 2015;112(38):E5361-E5370.

61. Mishra P, Narayanan R. Conjunctive changes in multiple ion channels mediate activity-dependent intrinsic plasticity in hippocampal granule cells. *iScience* 2022;25(3):103922.

62. Yang J, Shakil H, Ratté S, Prescott SA. Minimal requirements for a neuron to coregulate many properties and the implications for ion channel correlations and robustness. *eLife* 2022;11:e72875.

63. Ratté S, Zhu Y, Lee KY, Prescott SA. Criticality and degeneracy in injury-induced changes in primary afferent excitability and the implications for neuropathic pain. *eLife* 2014;3:e02370.

64. Drion G, Massotte L, Sepulchre R, Seutin V. How modeling can reconcile apparently discrepant experimental results: the case of pacemaking in dopaminergic neurons. *PLoS Comput Biol* 2011;7(5):e1002050.

65. Puopolo M, Raviola E, Bean BP. Roles of subthreshold calcium current and sodium current in spontaneous firing of mouse midbrain dopamine neurons. *J Neurosci* 2007;27(3):645–656.

66. Swensen AM, Bean BP. Robustness of burst firing in dissociated purkinje neurons with acute or long-term reductions in sodium conductance. *J Neurosci* 2005;25(14):3509–3520.

67. Knox AT, Glauser T, Tenney J, Lytton WW, Holland K. Modeling pathogenesis and treatment response in childhood absence epilepsy. *Epilepsia* 2018;59(1):135–145.

68. Prinz AA, Bucher D, Marder E. Similar network activity from disparate circuit parameters. *Nat Neurosci* 2004;7(12):1345–1352.

69. Grashow R, Brookings T, Marder E. Compensation for variable intrinsic neuronal excitability by circuit-synaptic interactions. *J Neurosci* 2010;30(27):9145–9156.

70. Medlock L et al. Multiscale computer model of the spinal dorsal horn reveals changes in network processing associated with chronic pain. *J Neurosci* 2022;42(15):3133–3149.

71. Prescott SA, Sejnowski TJ, De Koninck Y. Reduction of anion reversal potential subverts the inhibitory control of firing rate in spinal lamina I neurons: towards a biophysical basis for neuropathic pain. *Mol Pain* 2006;2:32.

72. Lee KY, Prescott SA. Chloride dysregulation and inhibitory receptor blockade yield equivalent disinhibition of spinal neurons yet are differentially reversed by carbonic anhydrase blockade. *Pain* 2015;156(12):2431–2437.

73. Campbell JN, Raja SN, Meyer RA, Mackinnon SE. Myelinated afferents signal the hyperalgesia associated with nerve injury. *Pain* 1988;32(1):89–94.

74. Koltzenburg M, Lundberg LE, Torebjork HE. Dynamic and static components of mechanical hyperalgesia in human hairy skin. *Pain* 1992;51(2):207–219.

75. Liu C-N et al. Tactile allodynia in the absence of C-fiber activation: altered firing properties of DRG neurons following spinal nerve injury. *Pain* 2000;85(3):503–521.

76. Liu X, Eschenfelder S, Blenk KH, Janig W, Habler H. Spontaneous activity of axotomized afferent neurons after L5 spinal nerve injury in rats. *Pain* 2000;84(2–3):309–318.

77. Shields SD et al. Insensitivity to pain upon adult-onset deletion of $Na_V1.7$ or its blockade with selective inhibitors. *J Neurosci* 2018;38(47):10180–10201.

78. Abrahamsen B et al. The cell and molecular basis of mechanical, cold, and inflammatory pain. *Science* 2008;321(5889):702–705.

79. Minett MS et al. Pain without nociceptors? $Na_V1.7$-independent pain mechanisms. *Cell Rep* 2014;6(2):301–12.

80. Goaillard JM, Marder E. Ion channel degeneracy, variability, and covariation in neuron and circuit resilience. *Annu Rev Neurosci* 2021;44:335–357.

81. Schild JH, Kunze DL. Experimental and modeling study of Na^+ current heterogeneity in rat nodose neurons and its impact on neuronal discharge. *J Neurophysiol* 1997;78(6):3198–3209.

82. Blair NT, Bean BP. Roles of tetrodotoxin (TTX)-sensitive Na^+ current, TTX-resistant Na^+ current, and Ca^{2+} current in the action potentials of nociceptive sensory neurons. *J Neurosci* 2002;22(23):10277–10290.

83. Malin SA, Davis BM, Molliver DC. Production of dissociated sensory neuron cultures and considerations for their use in studying neuronal function and plasticity. *Nat Protoc* 2007;2(1):152–160.

84. Davidson S et al. Human sensory neurons: Membrane properties and sensitization by inflammatory mediators. *Pain* 2014;155(9):1861–1870.

85. Elliott AA, Elliott JR. Characterization of TTX-sensitive and TTX-resistant sodium currents in small cells from adult rat dorsal root ganglia. *J Physiol* 1993;463:39–56.

86. Vasylyev D V, Han C, Zhao P, Dib-Hajj S, Waxman SG. Dynamic-clamp analysis of wild-type human $Na_V1.7$ and erythromelalgia mutant channel L858H. *J Neurophysiol* 2014;111(7):1429–1443.

87. Han C et al. Human $Na_V1.8$: enhanced persistent and ramp currents contribute to distinct firing properties of human DRG neurons. *J Neurophysiol* 2015;113(9):3172–3185.

88. Sundt D, Gamper N, Jaffe DB. Spike propagation through the dorsal root ganglia in an unmyelinated sensory neuron: a modeling study. *J Neurophysiol* 2015;114(6):3140–3153.

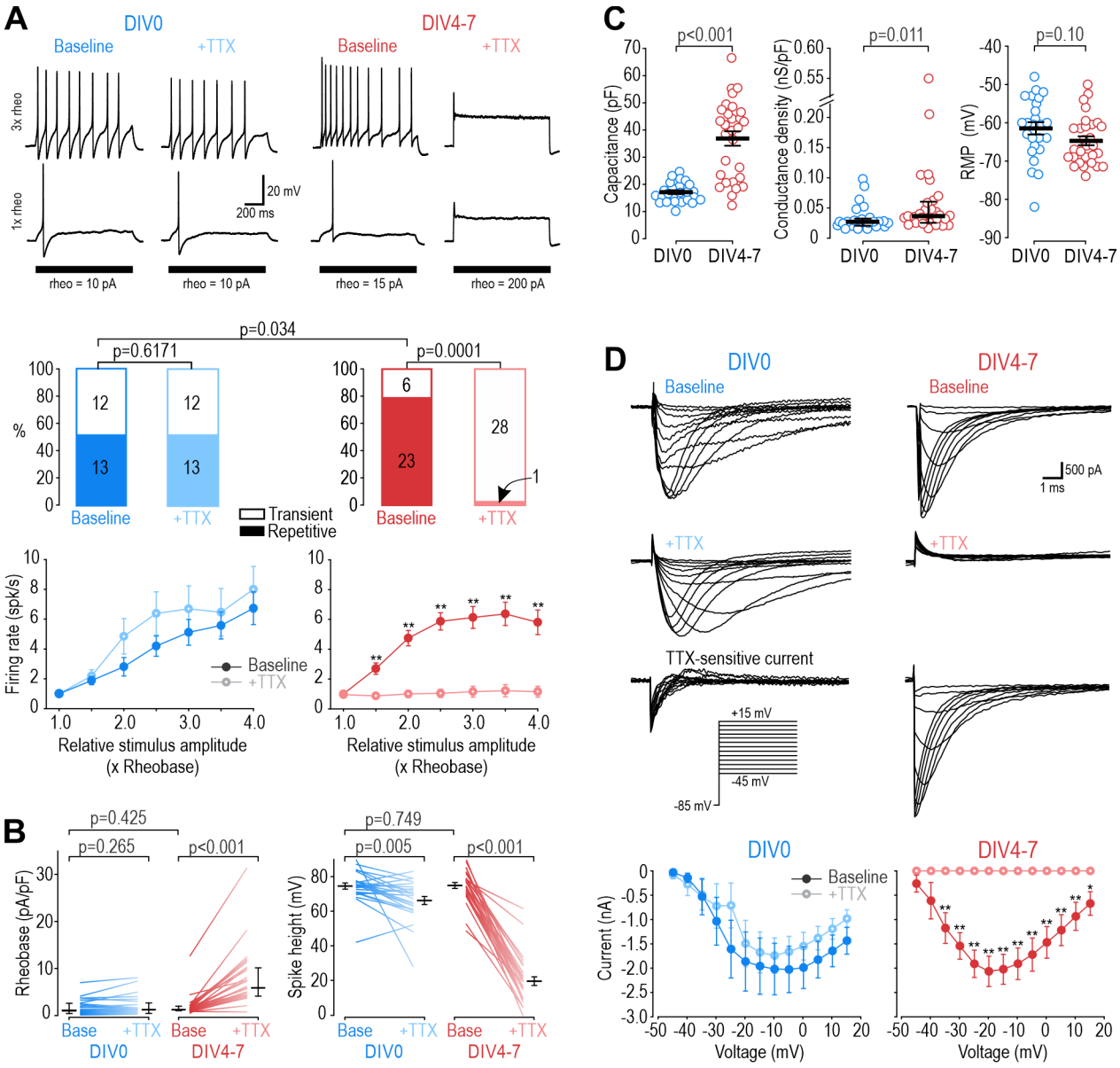

Figure 1. Different Na_V isoforms produce equivalent excitability at different days in vitro (DIV).

(A) Representative responses of small DRG neurons to current injection at rheobase and 3x rheobase when tested on DIV0 (blue) or DIV4-7 (red) before (dark) and after (pale) bath application of 100 nM TTX. At DIV0, TTX did not alter spiking pattern (χ^2=0.25, p=0.617, McNemar test) or significantly reduce firing rate ($F_{1,72}$=1.527, p=0.24, two-way repeated measure (RM) ANOVA; n=13). At DIV4-7, TTX significantly altered spiking pattern, converting all but one neuron to transient spiking (χ^2=20.05, p<0.0001), and it significantly reduced firing rate ($F_{1,132}$=43.157, p<0.001, n=23). Only neurons with repetitive spiking at baseline are included in the firing rate plot. **(B)** At DIV0, TTX did not affect rheobase (Z_{24}=1.129, p=0.265, Wilcoxon rank test) but did reduce spike height (T_{24}=3.092, p=0.005, paired t-test). At DIV4-7, TTX

increased rheobase (Z_{28}=4.681, p<0.001, Wilcoxon rank test) and dramatically reduced spike height (T_{28}=20.333, p<0.001, paired t-test). Notably, neurons at DIV0 and DIV4-7 did not differ in their baseline rheobase (U=316, p=0.425, Mann-Whitney test) or spike height (T_{52}=0.322, p=0.749, t-test). **(C)** Neurons at DIV0 and DIV4-7 differed in their total capacitance (T_{52}=6.728, p<0.001, t-test) and leak conductance density (U=216, p=0.011, Mann-Whitney test) but not in their resting membrane potential (T_{52}=1.668, p=0.101, t-test). **(D)** Sample voltage clamp recordings with command voltage stepped from -85 mV to +15 mV in 5 mV increments, before and after TTX. Sodium current was not significantly reduced by TTX at DIV0 ($F_{1,72}$=3.585, p=0.107, two-way RM ANOVA; n=7 neurons) but was completely abolished by TTX at DIV4-7 ($F_{1,108}$=33.526, p<0.001; n=10 neurons). *, p<0.05; **, p<0.01; Student- Newman-Keuls post-hoc tests in A and D.

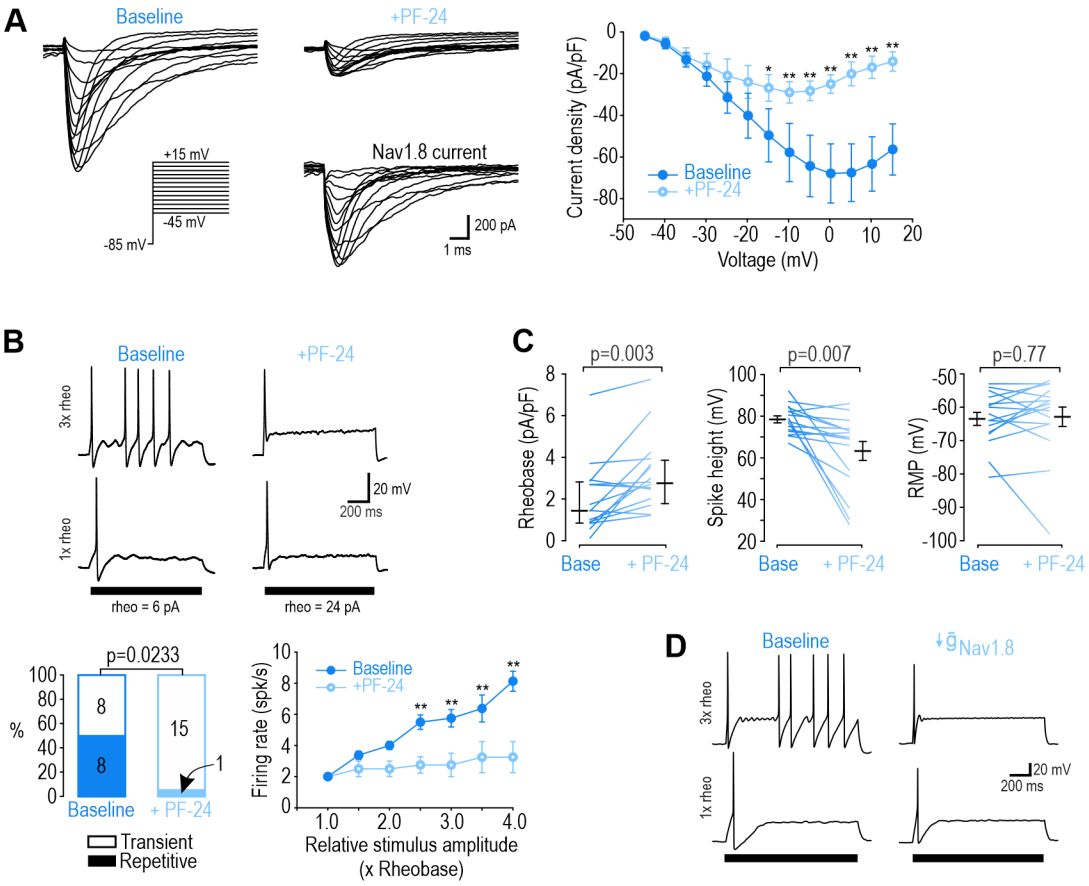

Figure 2. $Na_V1.8$ is necessary for repetitive spiking at DIV0.

(A) Sample voltage clamp recordings show that sodium current was almost completely abolished by the $Na_V1.8$ inhibitor PF-24 (1 µM). Peak current was significantly reduced by PF-24 ($F_{1,72}$=12.651, p<0.012, two-way RM ANOVA; n=7). Another $Na_V1.8$ inhibitor, A-803467, had a similar effect (see Fig. S1). **(B)** PF-24 significantly altered spiking pattern (χ^2=5.14, p=0.0233, McNemar test) and reduced firing rate ($F_{1,42}$=11.946, p=0.011, two-way RM ANOVA; n=8). **(C)** PF-24 significantly increased rheobase (Z_{15}=2.783, p=0.003, Wilcoxon rank test) and reduced spike height (T_{15}=3.151, p=0.007, paired t-test) but did not affect resting membrane potential (T_{15}=0.304, p=0.765, paired t-test). The $Na_V1.7$ inhibitor PF-71 had negligible effects at DIV0 (see Fig. S3). **(D)** A computational model reproduced the effect of $Na_V1.8$ on spiking pattern (also see Supplementary Table 1). The PF-24 effect was simulated as a ~85% reduction in $Na_V1.8$ ($\bar{g}_{\mathrm{Nav1.8}}$= 4mS/cm2). *, p<0.05; **; p<0.01; Student-Newman-Keuls post-hoc tests in A and B.

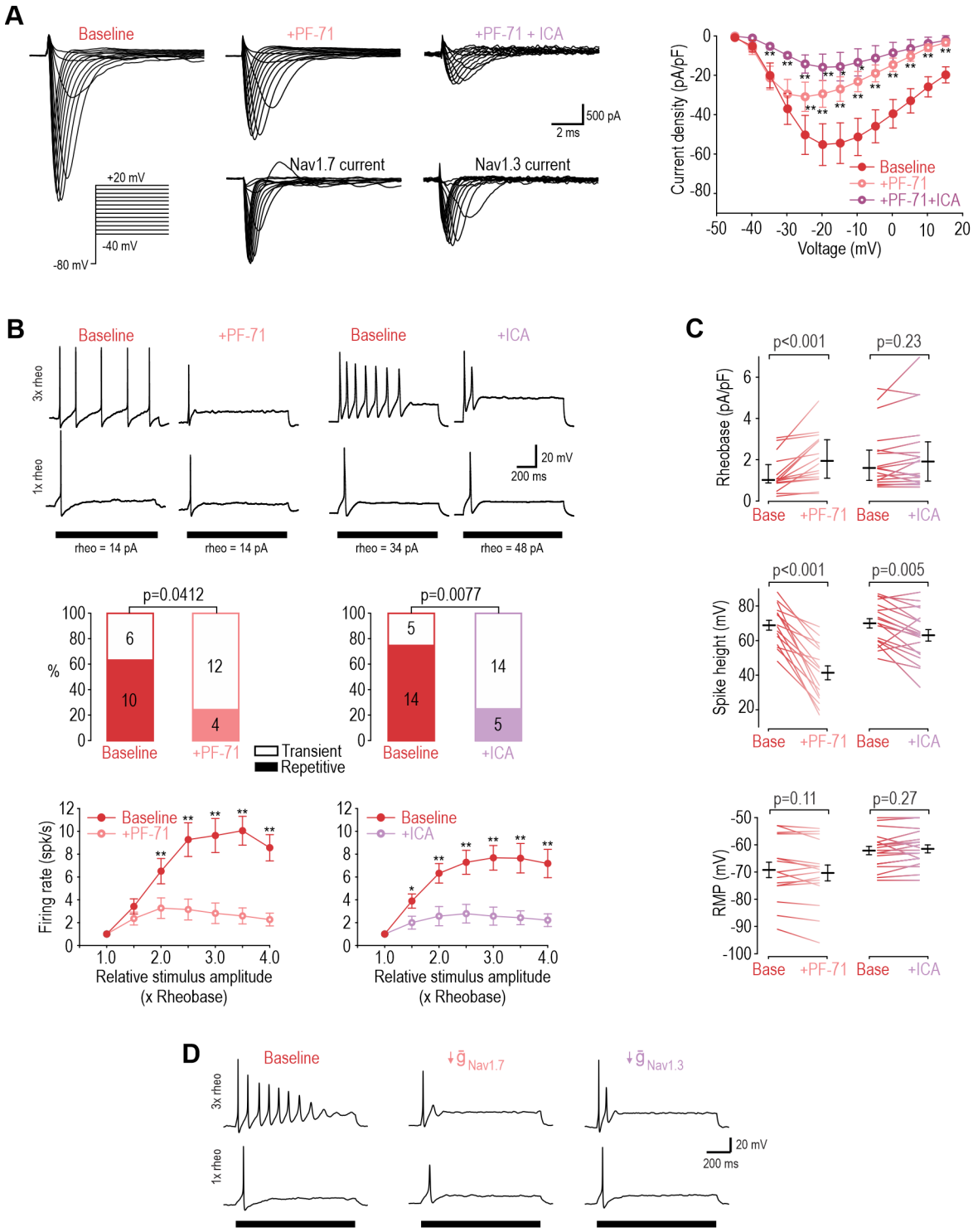

Figure 3. $Na_V1.3$ and $Na_V1.7$ are necessary for repetitive spiking at DIV4-7.

(A) Sample voltage clamp recordings show that sodium current was reduced by the $Na_V1.7$ inhibitor PF-71 (30 nM) and by the $Na_V1.1/1.3$ inhibitor ICA (1 µM). Peak current was significantly reduced by PF-71 and ICA ($F_{2,192}$=26.361, p<0.001, two-way RM ANOVA; n=9). **(B)** PF-71 and ICA both significantly altered

spiking pattern (χ^2=4.17, p=0.041 and χ^2 =7.11, p=0.0077, respectively, McNemar tests) and significantly reduced firing rate ($F_{1,54}$=40.659, p<0.001, n=10 and $F_{1,78}$=35.156, p<0.001, n=14, respectively, two-way RM ANOVAs). **(C)** PF-71 significantly increased rheobase (Z_{18}=3.464, p<0.001, Wilcoxon rank test) and decreased spike height (T_{18}=7.946, p<0.001, paired t-test). ICA did not significantly alter rheobase (Z_{18}=1.248, p=0.225) but did reduce spike height (T_{18}=3.243, p=0.005). Neither drug affected resting membrane potential (T_{15}=1.681, p=0.113 for PF-71; T_{18}=-1.132, p=0.272 for ICA, paired t-test). The $Na_V1.8$ antagonist PF-24 had negligible effects at DIV4-7 (see Fig. S2). **(D)** A computational model reproduced the combined effects of $Na_V1.3$ and $Na_V1.7$ on spiking pattern (also see Supplementary Table 1). PF-71 effect was simulated as a 70% reduction in $Na_V1.7$ ($\bar{g}_{\mathrm{Nav1.7}}$= 10.5 mS/cm^2). ICA effect was simulated as a 90% reduction in $Na_V1.3$ ($\bar{g}_{\mathrm{Nav1.3}}$= 0.035 mS/cm^2). *, p<0.05; **, p<0.01; Student-Newman-Keuls post-hoc tests in A and B.

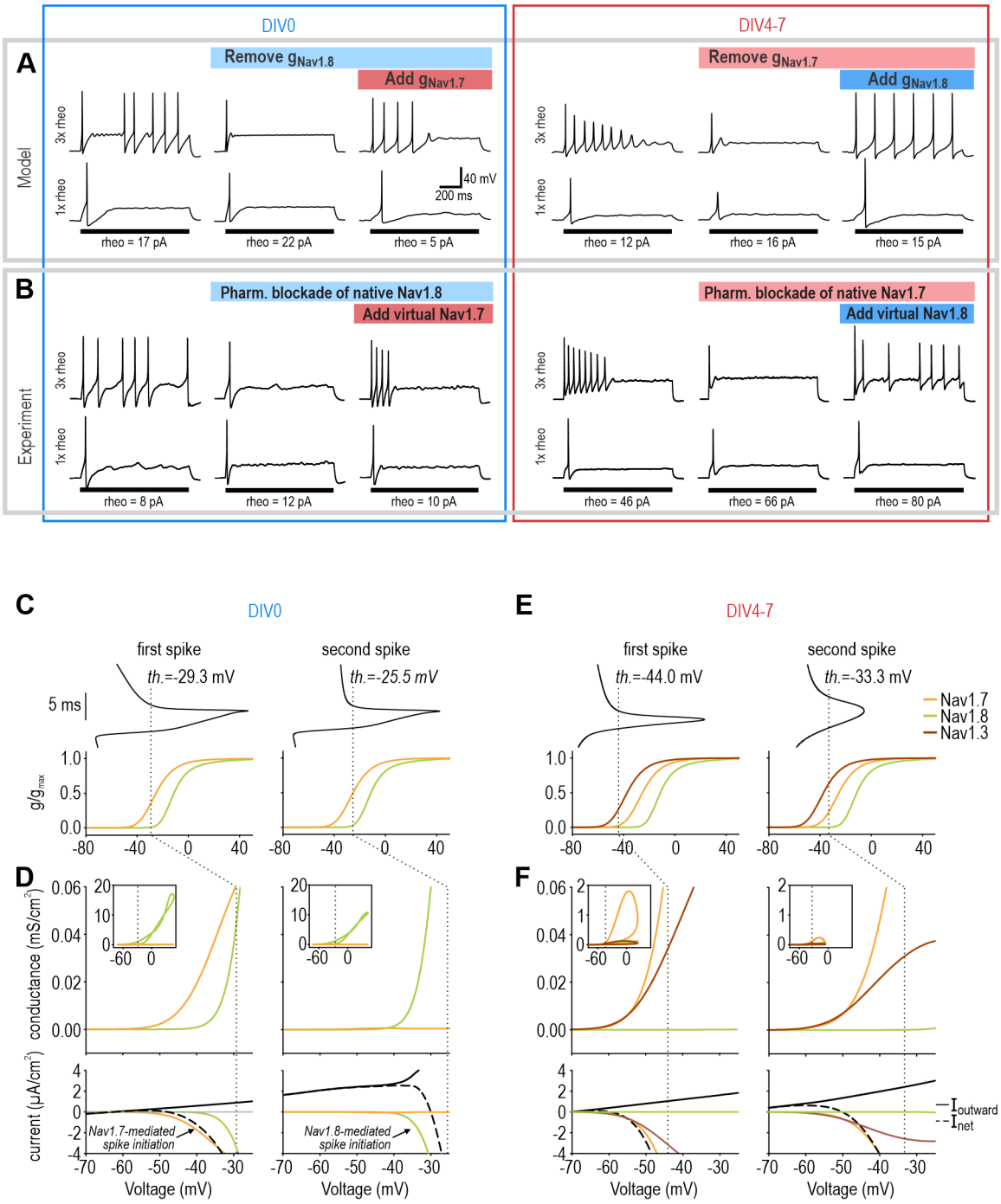

Figure 4. $Na_V1.7$ and $Na_V1.8$ are each sufficient to produce repetitive spiking in DIV0 and DIV4-7 neurons. (A) The computational model predicts that the $Na_V1.8$ conductance, which is "necessary" for repetitive spiking at DIV0 can, in principle, be replaced by $Na_V1.7$ (left), and vice versa at DIV4-7 (right). **(B)** Replacement experiments involved inhibiting native channels pharmacologically and then introducing virtual conductances using dynamic clamp. At DIV0 (left), inhibiting native $Na_V1.8$ (with PF-24) converted neurons to transient spiking, but introducing virtual $Na_V1.7$ reverted neurons to repetitive spiking (in 3 of

3 neurons tested). At DIV4-7, inhibiting native $Na_V1.7$ (with PF-71) converted the neuron to transient spiking, but introducing virtual $Na_V1.8$ reverted neurons to repetitive spiking (in 4 of 4 neurons tested). Parameters for virtual channels were identical to simulations except for the maximal conductance density, which was titrated in each cell. **(C)** Voltage (top) for first (left) and second (right) spikes in the DIV0 model aligned with voltage activation curves for each Na_V isoform (bottom). Dashed line shows voltage threshold (defined as V where dV/dt reaches 5 mV/ms). **(D)** Conductance plotted against voltage to create a phase portrait (top) showing Na_V conductance at different phases of the spike. Inset shows full voltage range; main graph zooms in on voltages near threshold. Bottom plots show current plotted over the same voltage range. For the first spike, $Na_V1.7$ (orange) mediates nearly all perithreshold inward current. For the second spike, voltage threshold is increased and $Na_V1.8$ (green) mediates nearly all perithreshold inward current because $Na_V1.7$ has inactivated (see Fig. S6). (**E-F**) In the DIV4-7 model, $Na_V1.7$ (orange) and $Na_V1.3$ (maroon) contribute to initiation of all spikes whereas the contribution of $Na_V1.8$ is negligible.

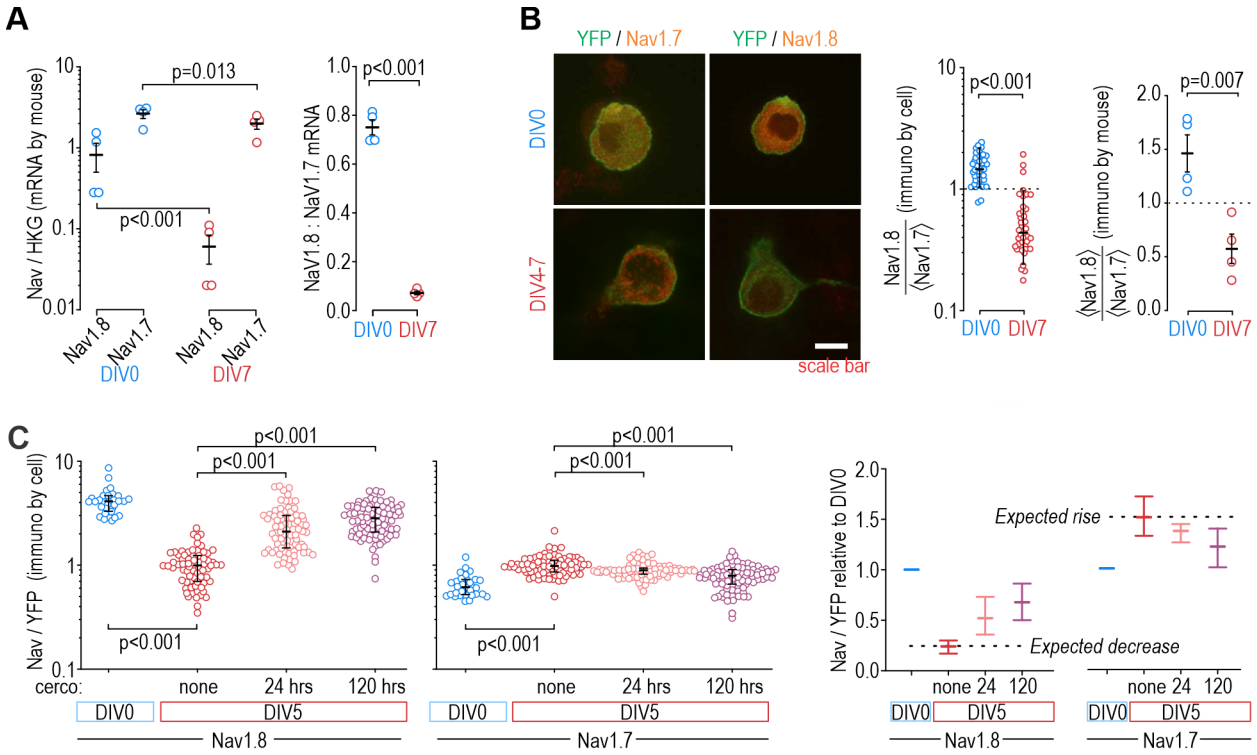

Figure 5. Protein levels, but not mRNA, reflect functional contributions of Na_V isoforms at DIV0 and DIV7.

(A) Both $Na_V1.8$ and $Na_V1.7$ mRNA levels (relative to a housekeeping gene (HKG), see Methods) decreased significantly between DIV0 and DIV4-7 (factor 1: time, $F_{1,12}$=56.677, p<0.001, factor 2: Na_V isoform, $F_{1,12}$=17.952, p=0.001, two-way ANOVA and Student-Newman-Keuls post-hoc tests on log transformed data, n=4 mice per time point) but more so for $Na_V1.8$ than for $Na_V1.7$ (interaction: time x isoform, $F_{1,12}$= 11.455, p=0.005). The differential reduction translated into a significantly higher $Na_V1.8$: $Na_V1.7$ ratio on DIV0 than at DIV4-7 (T_6=21.375, p<0.001, unpaired t-test). These changes may account for $Na_V1.8$ becoming unnecessary for repetitive spiking at DIV4-7 but cannot account for $Na_V1.7$ becoming necessary. **(B)** Immunoreactivity (IR) for $Na_V1.8$ protein exceeded $Na_V1.7$-IR at DIV0, but the opposite was true on DIV4-7. Na_V-IR was measured relative to YFP-IR in the same cell, and then each cell's $Na_V1.8$:YFP ratio was considered relative to the average $Na_V1.7$:YFP ratio in the co-processed coverslip (left) or average $Na_V1.8$:YFP ratio was considered relative to the average $Na_V1.7$:YFP ratio in the same animal (right). Both ratios were >1 at DIV0 but decreased significantly at DIV4-7 (U=78, p<0.001, n=37 for DIV0, n=40 for DIV4-7, Mann-Whitney test (left) and T_6=4.046, p=0.007, unpaired t-test (right)). **(C)** Chronically applied cercosporamide (10 µM) mitigated the changes in $Na_V1.8$- and $Na_V1.7$-IR at DIV5 ($Na_V1.8$: H_3=157.95, p<0.001; $Na_V1.7$: H_3=80.662, p<0.001; One-way ANOVA on ranks, Dunn's post-hoc tests, p<0.05 for all pairs). Panel on the right shows data normalized to baseline (DIV0) to emphasize relative changes.

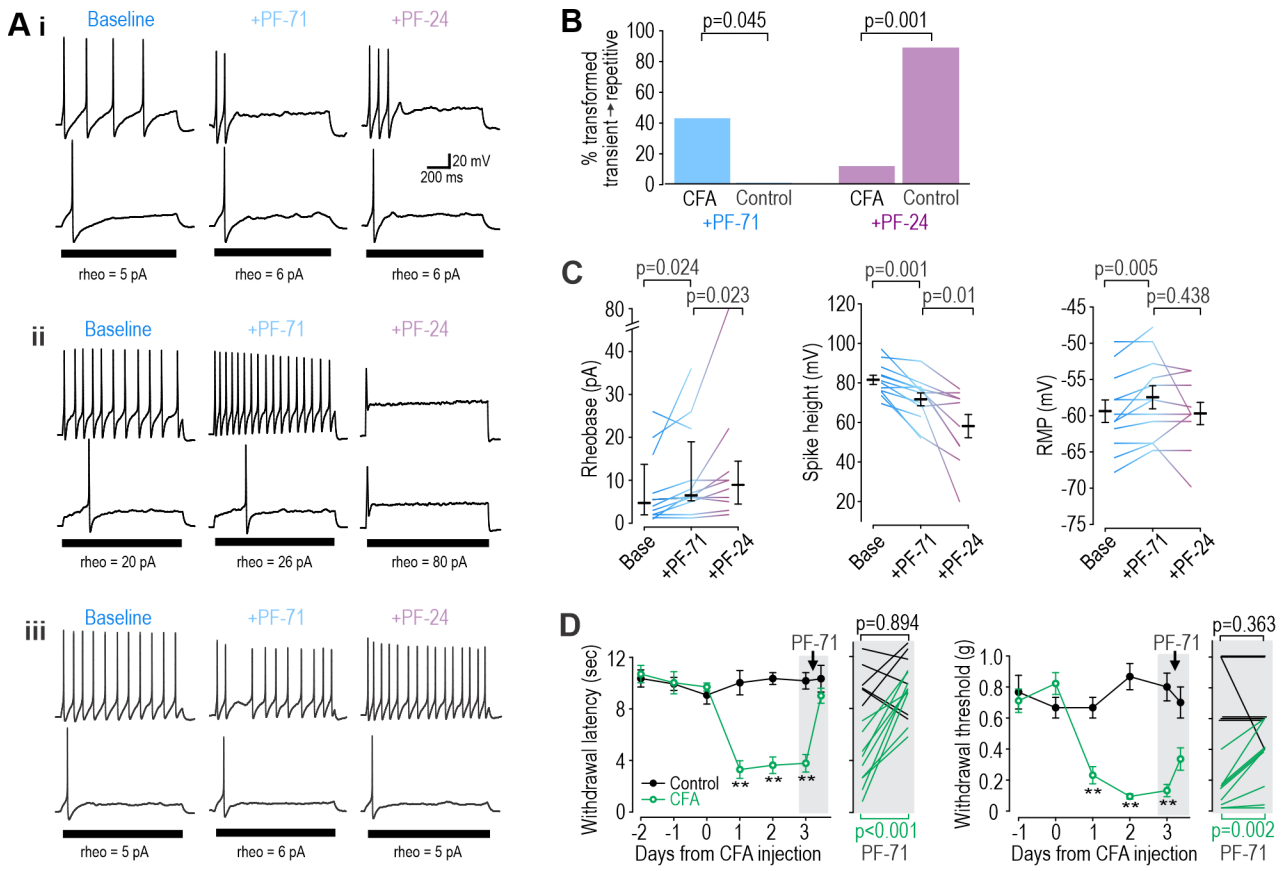

Figure 6. Inflammation alters Na_V isoform contribution to nociceptor excitability, with implications for analgesic efficacy.

(**A**) Sample responses in DIV0 neurons from mice injected with CFA three days earlier. In 12 cells tested, PF-71 converted 5 neurons to transient spiking (**i**), encouraged repetitive spiking in 4 neurons (**ii**), and had no effect in 3 neurons (**iii**), thus highlighting increased heterogeneity after CFA. (**B**) At DIV0, the effect of PF-71 differed significantly between CFA and control neurons, converting 42% (5 of 12) CFA neurons from repetitive to transient spiking vs 0% (0 of 9) control neurons (p=0.0451, Fisher Exact test)**.** Applying PF-24 to neurons that continued to spike repetitively after PF-71 had little effect on CFA neuron, converting only 13% (1 of 7) of CFA neurons vs 88% (7 of 8) of control neurons (p=0.001, Fisher Exact test). Together these results argue that $Na_V1.7$ contributes more and $Na_V1.8$ contributes less to nociceptor excitability after inflammation. **(C)** At DIV0, PF-71 significantly increased resting membrane potential (T_{11}=-3.530, p=0.005, paired t-test) and rheobase (Z_{11}=2.186, p=0.024, Wilcoxon rank test), and significantly decreased spike height (T_{11}=4.413, p=0.001, paired t-test) in CFA neurons. Further addition of PF-24 significantly changed rheobase (Z_9=2.176, p=0.023, Wilcoxon rank test) and action potential amplitude (T_9=3.237, p=0.01, paired t-test) but did not affect resting membrane potential (T_9=1.049, p=0.321, paired t-test). **(D)** Paw inflammation caused by CFA significantly altered thermal sensitivity (Hargreaves: $F_{5,65}$=19.556, p<0.001,

two-way RM ANOVA) and mechanical sensitivity (von Frey: $F_{4,52}$=16.786, p<0.001). When given three days after CFA, PF-71 significantly reversed the altered sensitivities (Hargreaves: T_8=-7.296, p<0.001; von Frey: T_8=-4.341, p=0.002; paired t-tests) but had no effect in naive mice (Hargreaves: T_5=-0.141, p=0.894; von Frey: T_5=1.000, p=0.363). Insets show values for each animal before and 2 hours after PF-71 injection. *, p<0.05; **, p<0.01; Student-Newman-Keuls post-hoc tests.

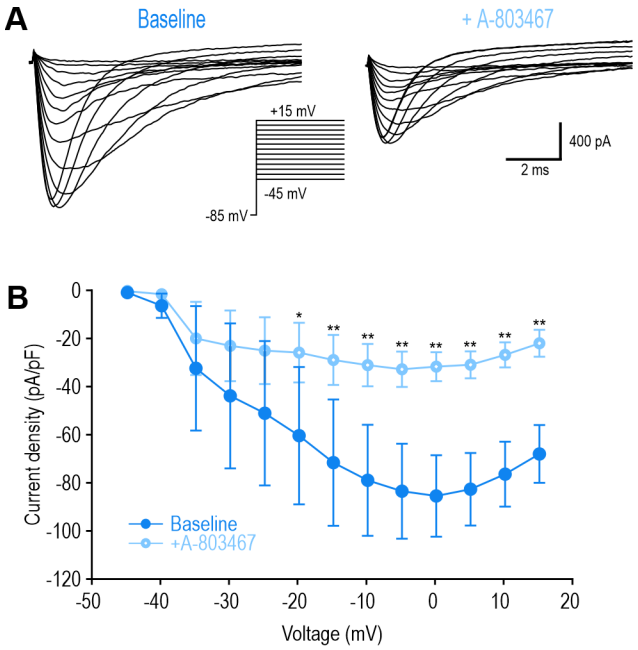

Figure S1. Inhibiting $Na_V1.8$ at DIV0 with a different antagonist, A-803467, had the same effect as PF-24. **(A)** Sample voltage clamp recording at DIV0 before and after A-803467 (1 µM). **(B)** Peak current was significantly reduced by A-803467 ($F_{1,84}$=9.935, p=0.016, two-way RM ANOVA, n=8). *, p<0.05; **, p<0.01; Student-Newman-Keuls post-hoc test in B.

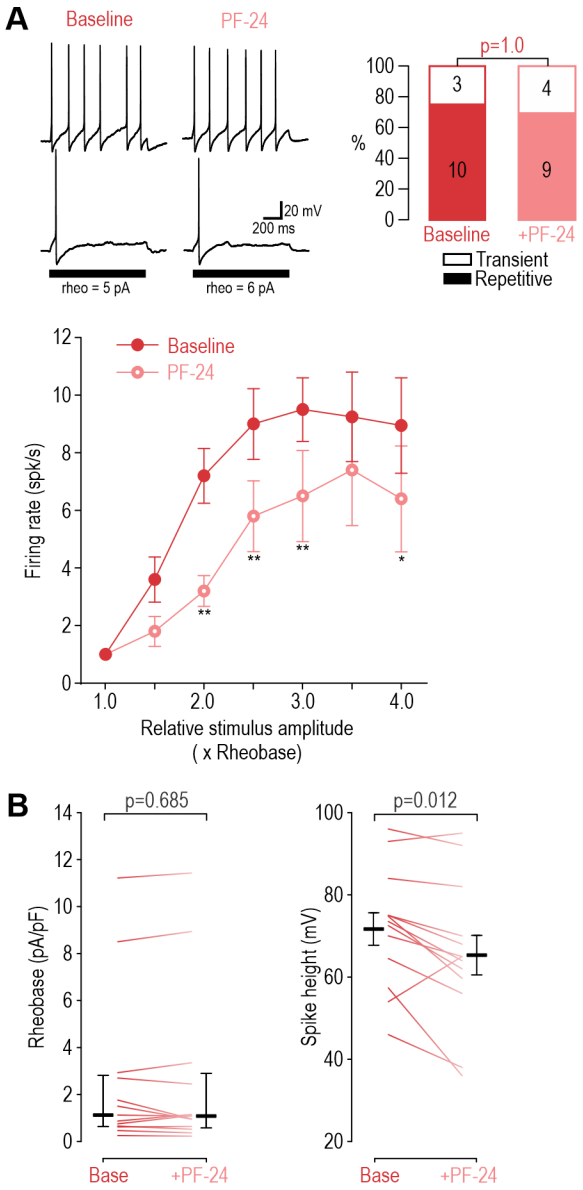

Figure S2. Inhibiting $Na_V1.8$ at DIV4-7 had limited effects.

(A) Inhibiting $Na_v1.8$ with PF-24 (1 µM) did not affect spiking pattern (χ^2 =0.00, p=1.00, McNemar test) and modestly reduced firing rate ($F_{1,54}$=9.745, p= 0.012, two-way RM ANOVA, n=10) in DIV4-7 neurons. **(B)** PF-24 did not affect rheobase (Z_{12}=0.420, p=0.685, Wilcoxon Rank test) but did reduce spike height (T12=2.939, p=0.012, paired-t-test). *, p<0.05; **, p<0.01; Student-Newman-Keuls post-hoc tests in A.

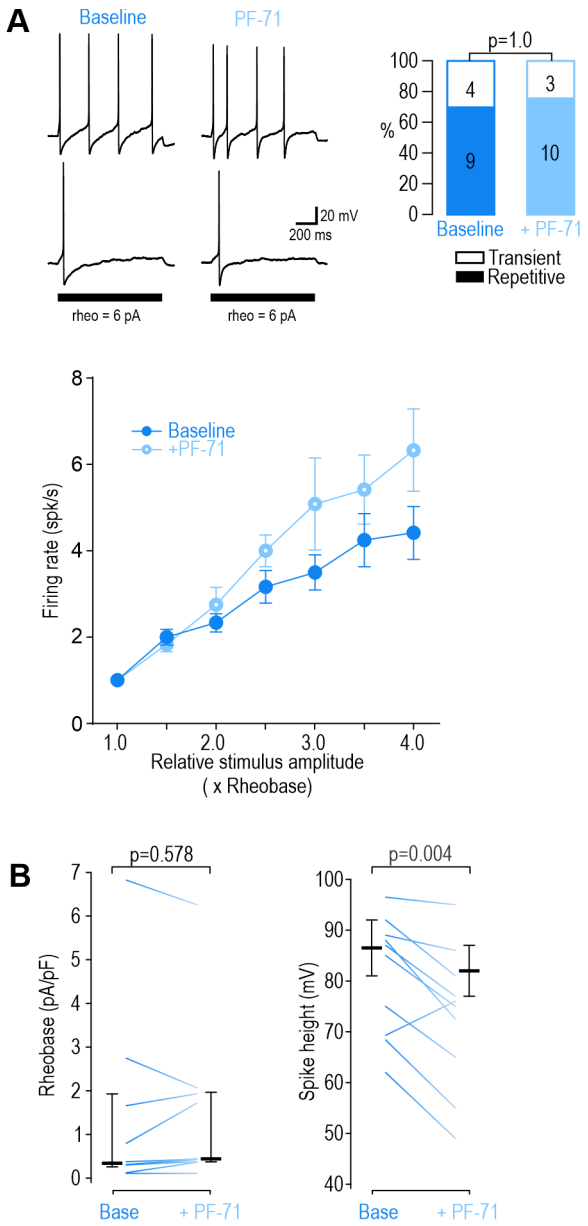

Figure S3. Inhibiting $Na_V1.7$ at DIV0 had limited effects.

(A) Inhibiting $Na_V1.7$ with PF-71 (30 nM) did not alter spiking pattern (χ^2=0.00, p=1.00, McNemar test) or reduce firing rate ($F_{1,30}$=5.805, p=0.061, two-way RM ANOVA, n=6) in DIV0 neurons; in fact, firing rate was slightly increased. **(D-E)** PF-71 did not affect rheobase (Z_9=0.677, p=0.578, Wilcoxon rank test) but did reduce spike height (T_9=3.759, p=0.004, paired-t-test).

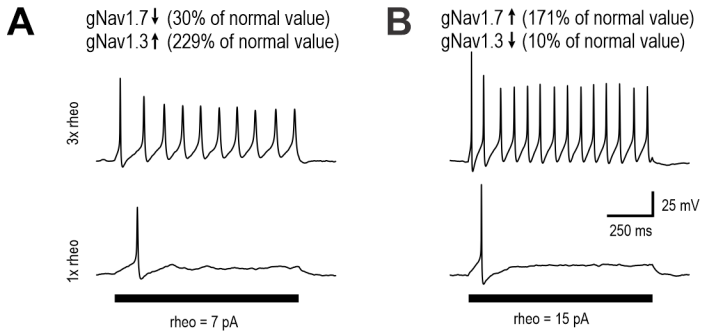

Figure S4. Na_V1.7 and Na_V 1.3 currents can compensate for each other and maintain repetitive spiking. **(A)** In the DIV4-7 model, reducing $\bar{g}_{\mathrm{Nav1.7}}$ to 30% of its normal value (35→10 mS/cm^2) can be compensated for by increasing $\bar{g}_{\mathrm{Nav1.3}}$ to 229% of its normal value (0.35→0.8 mS/cm^2) to maintain repetitive spiking. **(B)** Conversely, reducing $\bar{g}_{\mathrm{Nav1.3}}$ to 10% of its normal value (0.35→0.035 mS/cm^2) can be compensated for by increasing $\bar{g}_{\mathrm{Nav1.7}}$ to 171% of its normal value (35→60 mS/cm^2) and maintain repetitive spiking.

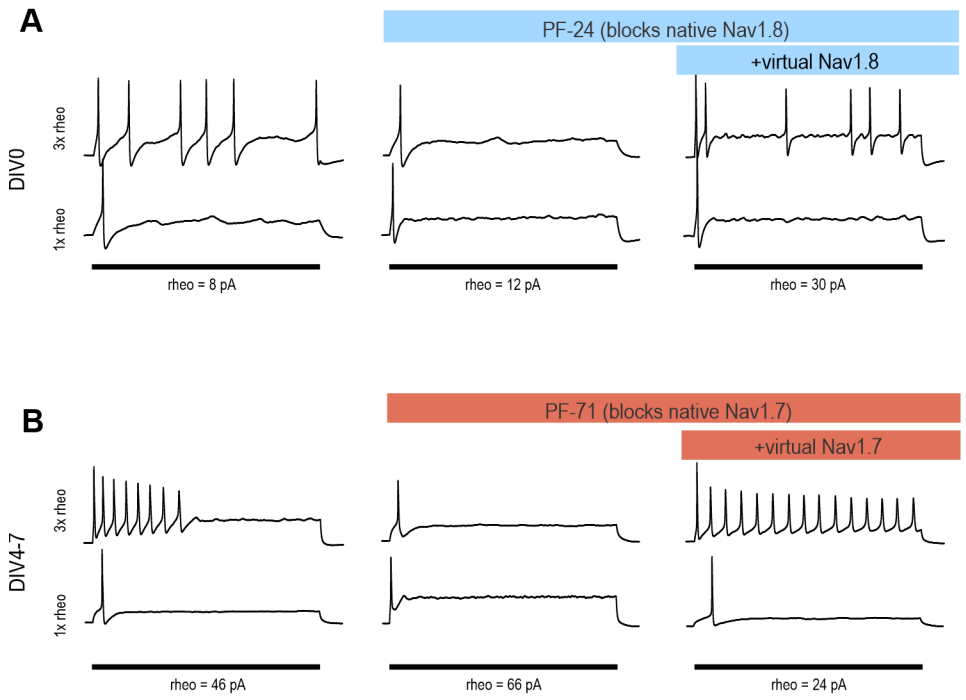

Figure S5. Virtual conductances restored repetitive spiking after pharmacological inhibition of the corresponding native conductance had converted the neuron to transient spiking.

(A) Sample response at DIV0 showing that a virtual $Na_V1.8$ conductance applied with dynamic clamp restored repetitive spiking after inhibiting native $Na_V1.8$ channels with PF-24. This restoration was repeated in 3 of 3 neurons tested. **(B)** Sample recording at DIV4-7 showing that a virtual $Na_V1.7$ conductance restored repetitive spiking after inhibiting native $Na_V1.7$ channels with PF-71. This restoration was repeated in 4 of 4 neurons tested.

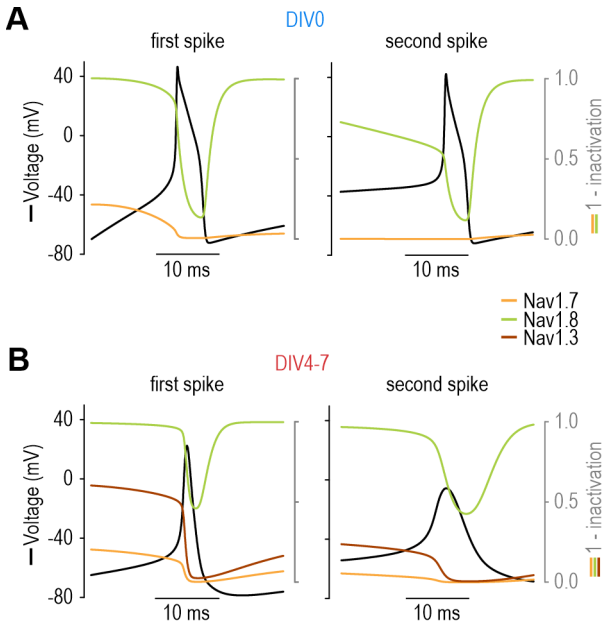

Figure S6. Channel inactivation contributes to isoform dependency for repetitive spiking.

(A) In the DIV0 model, $Na_V1.7$ contributed to the first spike but its inactivation meant that all subsequent spikes relied exclusively on $Na_V1.8$. **(B)** In the DIV4-7 model, despite some inactivation of $Na_V1.3$ (red) and $Na_V1.7$ (green), the remaining current was still large enough to produce a net inward current sufficient to support repetitive spiking.

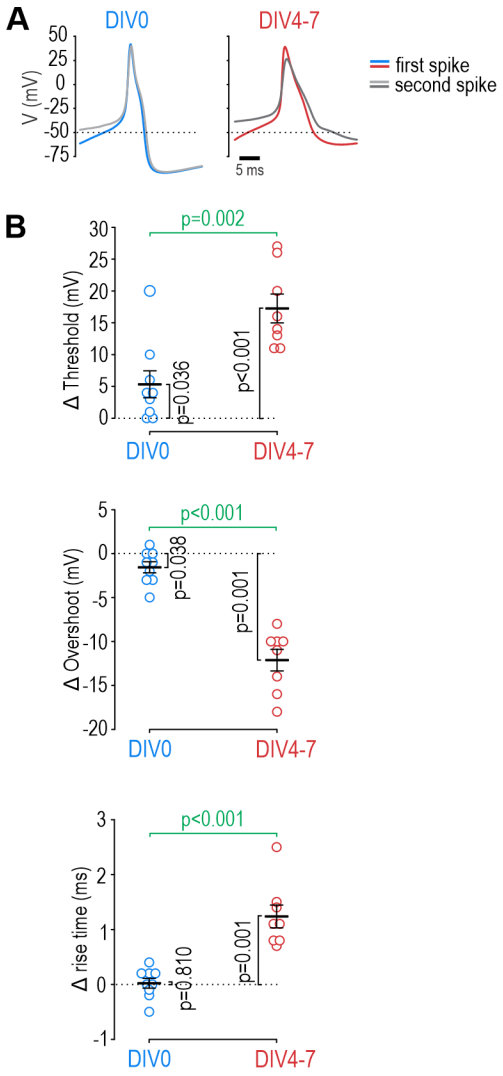

Figure S7. Differences in first and second spikes characteristics in experimental data.

Sample traces showing differences in the first (blue/red) and second (grey) spikes at DIV0 and DIV4-7. (**B**) Plots show differences (Δ) in threshold, overshoot potential, and spike rise time between 1st and 2nd spikes [spike 2 – spike 1] in a series of spikes triggered by current injection. At DIV0, the 1st and 2nd spikes differ significantly in their threshold (T_8=2.522, p=0.036, one-sample t-test) and overshoot (T_8=0.038, p=0.038) but not rise time (T_8=0.249, p=0.810). At DIV4-7, the 1st and 2nd spikes differ in all measures (threshold: T_7=7.613, p<0.001; overshoot: T_7=-9.849, p<0.001; rise time: T_7=5.979, p<0.001). Statistical results shown in green show that differences between 1st and 2nd spike at DIV4-7 are significantly larger than differences at DIV0 (threshold: T_{15}=-3.847, p=0.002; overshoot: T_{15}=7.922, p<0.001; rise time: T_{15}=-5.617, p<0.001, unpaired t-tests), consistent with our computational model.

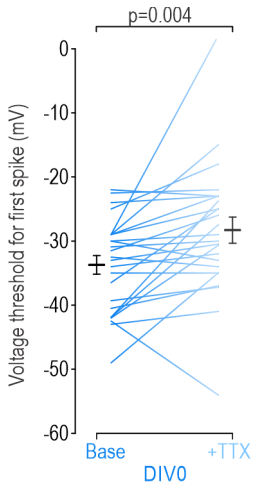

Figure S8. Effect of TTX on voltage threshold in DIV0 neurons.

Despite TTX having negligible effects in DIV0 neurons according to our initial analysis (see Fig. 1), simulation results in Fig. 4C-D predicted that the first spike was nonetheless initiated by $Na_V1.7$. By extension, this predicted that TTX should cause a depolarizing shift in voltage threshold for the first spike. Analysis of the experimental data confirmed this to be true, with threshold (mean±SEM) increasing from -33.7±1.4 mV at baseline to -28.3±1.4 mV after TTX (T_{24}=-3.19, p=0.004, paired t-test). Confirmation of this unexpected prediction helps further validate our model neuron.

Supplementary Table 1. Model data before and after channel "inhibition"

	DIV0		DIV4-7		
	Baseline	↓$Na_V1.8$	Baseline	↓$Na_V1.7$	↓$Na_V1.3$
Rheobase (pA)	17	22	12	16	21
Spike height (mV)	72.8	46.9	57.1	21.4	52
RMP (mV)	-69.0	-69.7	-70.0	-69.8	-70.4

Supplementary Table 2. Reagents

Reference term	Description	Concentration used	Source
TTX	Tetrodotoxin citrate	100 µM	Alomone, Israel
PF-24	PF-01247324	1 µM	Sigma, USA
PF-71	PF-05089771	30 nM	Alomone, Israel
ICA	ICA-121431	1 µM	Tocris, USA
Papain	Papain lyophilized power	27u/ml	Worthington
Collagenase	Collagenase type II	4mg/ml	Worthington
Dispase II	Dispase type II	4.7mg/ml	Sigma

Supplementary Table 3. Primers

	HPRT	$Na_V1.7$	$Na_V1.8$
NCBI Reference Sequence	*NM_013556.2*	*NM_001290674.1*	*NM_001205321.1*
Length	144	114	148
Forward	TCCTCCTCAGACCGCTTT	TGATGGTCATGGTGATTGGG	AGCCATCAAAGTGTCCGTC
Reverse	TTTTCCAAATCCTCGGCATAATG	TGTTTGCGTCGGTGTCTTC	CTTTATCAGAGCCTCGAAGGTG

Supplementary Table 4. Model equations

Channel Model	Equations
$Na_V1.7(86)$	$I_{NaV1.7} = \bar{g}_{NaV1.7} m^3 h (V - E_{Na})$ $\dot{m} = \alpha_m(1-m) - m\beta_m$ $\quad$ $\dot{h} = \alpha_h(1-h) - h\beta_h$ $\alpha_m = 10.22 - \frac{10.22}{1+\exp\left(\frac{V+7.19}{15.43}\right)}$ $\quad$ $\alpha_h = \frac{0.0744}{1+\exp\left(\frac{V+99.76}{11.07}\right)}$ $\beta_m = \frac{23.76}{1+\exp\left(\frac{V+70.37}{14.53}\right)}$ $\quad$ $\beta_h = 2.54 - \frac{2.54}{1+\exp\left(\frac{V+7.8}{10.68}\right)}$
$Na_V1.3$*	$I_{NaV1.3} = \bar{g}_{NaV1.3} m^3 h (V - E_{Na})$ $\dot{m} = \alpha_m(1-m) - m\beta_m$ $\quad$ $\dot{h} = \alpha_h(1-h) - h\beta_h$ $\alpha_m = 10.22 - \frac{10.22}{1+\exp\left(\frac{V+7.19+12}{15.43}\right)}$ $\quad$ $\alpha_h = \frac{0.0744}{1+\exp\left(\frac{V+99.76}{11.07}\right)}$

	$\beta_m = \frac{23.76}{1+\exp\left(\frac{V+70.37+12}{14.53}\right)}$ $\beta_h = 2.54 - \frac{2.54}{1+\exp\left(\frac{V+7.8}{10.68}\right)}$
$Na_V1.8$(87)	$I_{NaV1.8} = \bar{g}_{NaV1.8} m^3 h (V - E_{Na})$ $\dot{m} = \alpha_m(1-m) - m\beta_m$ $\dot{h} = \alpha_h(1-h) - h\beta_h$ $\alpha_m = 7.21 - \frac{7.21}{1+\exp\left(\frac{V-0.063}{7.86}\right)}$ $\alpha_h = 0.003 + \frac{1.63}{1+\exp\left(\frac{V+68.5}{10.01}\right)}$ $\beta_m = \frac{7.4}{1+\exp\left(\frac{V+53.06}{19.34}\right)}$ $\beta_h = 0.81 - \frac{0.81}{1+\exp\left(\frac{V-11.44}{13.12}\right)}$
K_M(88)	$I_{KM} = \bar{g}_{KM} n (V - E_K)$ $\dot{n} = \frac{n_\infty - n}{\tau_n}$ $n_\infty = \frac{1000}{1+e^{-\frac{V+35}{5}}}$ $\tau_n = \frac{1000}{3.3e^{V+\frac{35}{10}} + e^{-\frac{V+35}{10}}}$
K_{dr}(88)	$I_{KA} = \bar{g}_{KA} n^3 l (V - E_K)$ $\dot{n} = \alpha_m(1-m) - m\beta_m$ $\dot{l} = \alpha_h(1-h) - h\beta_h$ $\alpha_n = \frac{e^{(-5\times10^{-3}\cdot(V+32)\cdot 9.648\times10^4)}}{2562.35}$ $\alpha_l = \frac{e^{(2\times10^{-3}\cdot(V+61)\cdot 9.648\times10^4)}}{2562.35}$ $\beta_n = \frac{e^{(-2\times10^{-3}\cdot(V+32)\cdot 9.648\times10^4)}}{2562.35}$ $\beta_l = \frac{e^{(-2\times10^{-3}\cdot(V+32)\cdot 9.648\times10^4)}}{2562.35}$
AHP**	$I_{AHP} = \bar{g}_{AHP} z (V - E_K)$ $\dot{z} = \frac{1}{1+e^{5-V/4}} - \frac{z}{100}$

* Modified from $Na_V1.7$: a hyperpolarizing shift of 12mV in V1/2 of activation gate, m
** Modified from (50)
Note that the $Na_V1.7$ and $Na_V1.8$ equations above do not include the liquid junction potential correction of 4.2 mV (86) and 5.3 mV (87), respectively, that were applied in the neuron model.

Supplementary Table 5. Conductance densities at baseline for DIV 0 and 4-7 models

	Conductance densities at baseline (mS/cm^2)						
	$\bar{g}_{Nav1.3}$	$\bar{g}_{Nav1.7}$	$\bar{g}_{Nav1.8}$	$\bar{g}_{Kdr}$	$\bar{g}_{M}$	$\bar{g}_{AHP}$	$\bar{g}_{Leak}$
DIV 0	0	3	30	3	0.05	3.5	0.025
DIV 7	0.35	35	0.2	3.5	0.5	2.5	0.035